Published by Institute of Physics Publishing for SISSA

Received: *March 31, 2006*
Accepted: *June 2, 2006*
Published: *June 26, 2006*

Quiver gauge theories at resolved and deformed singularities using dimers

Iñaki García-Etxebarria,[a] **Fouad Saad**[a] **and Angel M. Uranga**[b]

[a] *Instituto de Física Teórica, C-XVI, Universidad Autónoma de Madrid*
Cantoblanco, 28049 Madrid, Spain
[b] *TH Unit, CERN*
CH-1211 Geneve 23, Switzerland
E-mail: innaki.garcia@uam.es, fouad.saad@uam.es, angel.uranga@cern.ch, angel.uranga@uam.es

Abstract: The gauge theory on a set of D3-branes at a toric Calabi-Yau singularity can be encoded in a tiling of the 2-torus denoted dimer diagram (or brane tiling). We use these techniques to describe the effect on the gauge theory of geometric operations partially smoothing the singularity at which D3-branes sit, namely partial resolutions and complex deformations. More specifically, we describe the effect of arbitrary partial resolutions, including those which split the original singularity into two separated. The gauge theory correspondingly splits into two sectors (associated to branes in either singularity) decoupled at the level of massless states. We also describe the effect of complex deformations, associated to geometric transitions triggered by the presence of fractional branes with confinement in their infrared. We provide tools to easily obtain the remaining gauge theory after such partial confinement.

Keywords: D-branes, Supersymmetric gauge theory.

JHEP06(2006)055

Contents

JHEP06(2006)055

1. Introduction

The study of the $N = 1$ supersymmetric gauge theory on a stack of D3-branes probing a Calabi-Yau threefold conical singularity is a fruitful source of new insights into brane dynamics [1, 2], the AdS/CFT correspondence [3], and its extensions to non-conformal situations by the addition of fractional branes [4].

Although present techniques do not allow this analysis for a general singular Calabi-Yau,[1] several techniques have been successfully applied to the understanding of D3-branes

[1] For certain simple singularities (like complex cones over del Pezzo surfaces) which include some non-toric cases, general methods based on exceptional collections have been applied, see e.g. [5, 6].

at toric singularities: Partial resolutions (e.g. [7 – 9]), mirror symmetry (e.g. [10, 11]), un-Higgsing [12, 13], etc. These tools have provided precise checks of AdS/CFT for quiver conformal field theories [14 – 19], and interesting information on related non-conformal systems [20 – 25].

A recent great improvement in the study of the system of D3-branes at a toric singularity has been the introduction of the so-called brane tilings or dimer diagrams [26 – 30]. These techniques have provided new viewpoints on the D3-brane gauge theory (e.g. its moduli space, its Seiberg dualities,[2] etc.). In addition they lead to interesting mathematical implications, like the description of the system in the large volume regime via exceptional collections [35], or a generalization of the McKay correspondence [27].

One expects that, although not completely general, toric singularities are representative enough for the physics of D3-branes at general singularities.

One of the basic features of string theory at Calabi-Yau singularities is the existence of localized modes which can smooth out the singularity. When D3-branes are located at such singularities, a natural question is what is the gauge theory interpretation of these smoothings (in other words, how do the D-branes experience this smoothing). A first kind of smoothings corresponds to partial resolutions and are associated to Kahler parameters. It has been known for some time that these modes couple as Fayet-Iliopoulos terms to the D-brane gauge theory [2]. In concrete examples it has been shown that they hence trigger a partial Higgsing of the gauge theory reducing it to the gauge theory in the left-over singularity [7]. The observation that minimal partial resolutions (those removing a triangle from the toric diagram) admit a simple description in terms of brane tilings [27], suggests the existence of a simple description of general partial resolutions in this language. In this paper we provide such a description, in terms of dimer diagram concepts and directly on the gauge theory side (by providing the relevant Higgsing vevs associated to a partial resolution). Our results significantly improve the understanding of partial resolutions in the literature, and can be used to easily analyze complicated resolutions which e.g. split the original singularity into two singularities.

A second kind of smoothing corresponds to complex deformations. These are extremely interesting from the gauge theory viewpoint, since they are related to geometric transitions triggered by fractional branes which experience confinement at the infrared. The prototypical situation is the conifold singularity with fractional branes [4, 36], but similar behaviour has been discussed in more generality (see e.g. [37], and [38, 22] for general toric singularities).

In [22] the gauge theory process of confinement of a subset of gauge factors was translated in an ad hoc manner to the dimer diagram language. In this paper we provide a detailed description of the effect of these geometric transitions in the gauge theory, allowing us to derive simple dimer diagram rules to obtain the remaining theory after infrared confinement of the fractional brane gauge groups. Moreover, this description provides a new insight into the nature of other kinds of fractional branes, which are known not to confine and trigger a complex deformation, but rather remove the supersymmetric groundstate [23 – 25, 39].

[2] See [31 – 34] for earlier descriptions of Seiberg dualities for D3-branes at singularities.

JHEP06(2006)055

The two kinds of smoothings are most easily described in terms of the web diagrams of the toric singularity [40 – 42]. Our main tool in finding the gauge theory counterpart of these geometric operations is the close relation between the dimer diagrams and the web diagram of the associated singularity [29, 28].

The paper is organized as follows. In section 2 we review some aspects of the dimer diagram techniques to study the gauge theory on D3-branes at toric singularities. This section contains all the background material on dimers we need, so sections 3 and 4 can be read independently. In section 3 we describe the effect of a general partial resolution of the singularity on the gauge theory. In section 3.1 and 3.2 we work out several examples in detail, describing the effects of the partial resolution on the dimer diagram via simple operations in its zig-zag paths. In section 3.3 we translate the dimer diagram rules for partial resolution to explicit vevs for the gauge theory bi-fundamentals, triggering the corresponding Higgs mechanism. The proof of their flatness is postponed to appendix A. In section 3.4 we provide a different view on the dimer description of partial resolutions in terms of perfect matchings. Finally, in section 3.5 we discuss partial resolution in the presence of fractional branes, and possible obstructions. In section 4 we describe complex deformations as geometric transitions triggered by fractional branes with infrared confining behaviour. In section 4.1 and 4.2 we work out several examples in detail, describing the effect of such geometric transitions on the dimer diagram via simple operations on its zig-zag paths. In section 4.3 we describe the field theory interpretation of the complex deformation, and describe in terms of the dimer diagrams the gauge theory analysis of branes probing the confining theory. In section 4.4 we provide a different view of the complex deformation in the dimer[3] in terms of perfect matchings. Finally in section 5 we offer some final remarks.

2. Review of dimer diagrams

In this section we review some background material on dimer diagrams and their relevant to quiver gauge theories. Reviews of the mathematical aspects of dimers can be found in [43, 44].

2.1 Quiver gauge theories and dimer diagrams

The gauge theory of D3-branes probing toric threefold singularities is determined by a set of unitary gauge factors (of equal rank in the absence of fractional branes, which we do not consider for the moment), chiral multiplets in bi-fundamental representations, and a superpotential given by a sum of traces of products of such bi-fundamental fields. The gauge group and matter content of such gauge theories can be encoded in a quiver diagram, such as that shown in figure 1a, with nodes corresponding to gauge factors, and arrows to bi-fundamentals. The superpotential terms correspond to closed loops of arrows, but the quiver does not fully encode the superpotential.

[3]We will frequently abuse language and simply call *dimer* the complete dimer graph. Strictly speaking a dimer is what we call an edge.

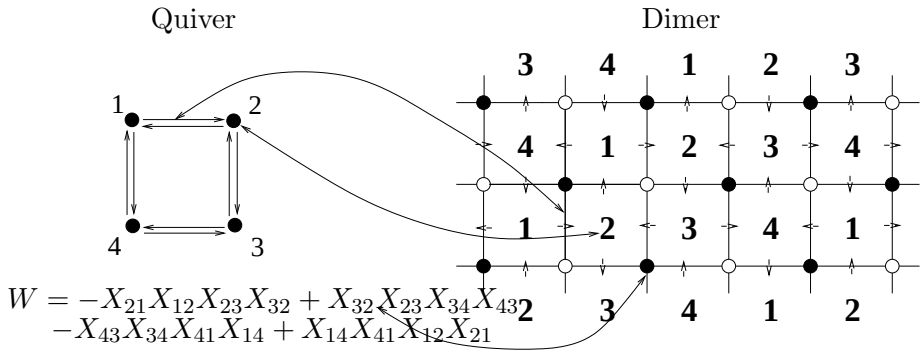

Figure 1: Quiver and dimer for a $\mathbf{Z_2}$ orbifold of the conifold. Faces in the dimer correspond to gauge groups, edges correspond to bifundamentals and each vertex corresponds to a superpotential term. Edges have an orientation determined by the coloring of the adjacent nodes.

Recently it has been shown that all the gauge theory information, including the gauge group, the matter content and the superpotential, can be encoded in a so-called brane tiling or dimer graph [26, 27].[4] This is a tiling of $\mathbf{T^2}$ defined by a bipartite graph, namely one whose nodes can be colored black and white, with no edges connecting nodes of the same color Ṫhe dictionary associates faces in the dimer diagram to gauge factors in the field theory, edges with bi-fundamental fields (fields in the adjoint in the case that the same face is at both sides of the edge), and nodes with superpotential terms. The bipartite character of the diagram is important in that it defines an orientation for edges (e.g. from black to white nodes), which determines the chirality of the bi-fundamental fields. Also, the color of a node determines the sign of the corresponding superpotential term.

The explicit mapping between this bipartite graph and the gauge theory, is illustrated in one example in figure 1. Many interesting features of the gauge theory have been described in terms of dimers by now.

2.2 Dimer diagrams and the mirror Riemann surface

There are two interesting ways to relate physically the dimer diagram with the gauge theory. As described in [27] the diagram can be considered to specify a configuration of NS5- and D5-branes, generalizing the brane box [45 – 47] and brane diamond models [48]. The NS5-branes extend in the 0123 directions and wrap a holomorphic curve in the 4567 directions. The D5-branes span the 012346 directions and are bounded by the NS branes in the 46 directions. These directions are compact and parametrize a torus. The NS branes thus generate a tiling of this $\mathbf{T^2}$, represented by a bipartite graph of the kind described above, hence the name brane tiling.

A second useful and more explicit viewpoint on correspondence between the gauge theory on D3-branes at toric singularities and dimer diagrams was provided in [29] by using mirror symmetry, as we now describe.[5] The mirror geometry to a Calabi-Yau singularity

[4]The brane tiling / dimer diagram can be dualized to an improved quiver diagram, the periodic quiver, which also encodes all this information.

[5]Earlier applications of mirror symmetry to D3-branes at singularities can be found in [10, 11].

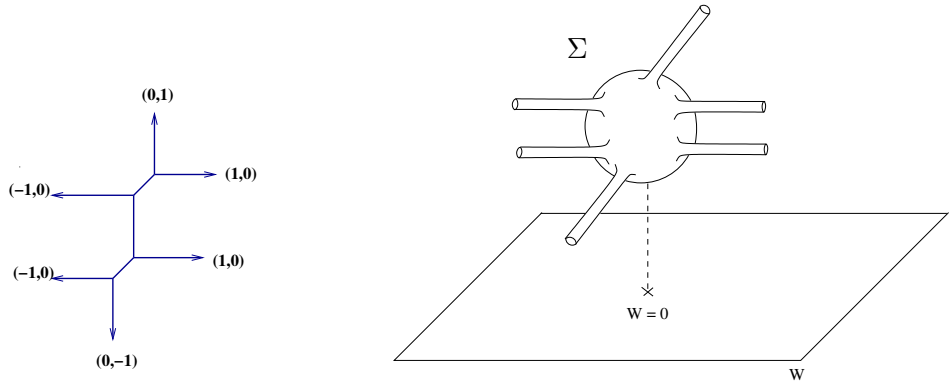

Figure 2: a) An example of a web diagram (for the theory in figure 1); b) the corresponding Riemann surface Σ in the mirror geometry.

$\mathcal{M}$ is specified by a double fibration over the complex plane W given by

$$W = P(z, w) \tag{2.1}$$

$$W = uv \tag{2.2}$$

with $w, z \in \mathbf{C}^*$ and $u, v \in \mathbf{C}$. Here $P(z, w)$ is the Newton polynomial of the toric diagram of $\mathcal{M}$. The surface $W = P(z, w)$ describes a genus g Riemann surface Σ_W with punctures, fibered over W. The genus g equals the number of internal points of the toric diagram. The fiber over $W = 0$, denoted simply Σ, will be important for our purposes. It corresponds to a smooth Riemann surface which can be thought of as a thickening of the web diagram [40 – 42] dual to the toric diagram, see figure 2.

At critical points $W = W^*$, a cycle in Σ_W degenerates and pinches off. Also, at $W = 0$ the S^1 in $W = uv$ degenerates. One can use these degenerations to construct non-trivial 3-cycles in the mirror geometry as follows. Consider the segment in the W-plane which joins $W = 0$ with one of the critical points $W = W^*$, and fiber over it the $\mathbf{S^1}$ in $W = uv$ times the 1-cycle in Σ_W degenerating at $W = W^*$, see figure 3. The result is a 3-cycle with an $\mathbf{S^3}$ topology. The number of such degenerations of Σ_W, and hence the number of such 3-cycles, is given by twice the area of the toric diagram.

Mirror symmetry specifies that the different gauge factors on the D3-branes in the original singularity arise from D6-branes wrapping the different 3-cycles. The 3-cycles on which the D6-branes wrap intersect over $W = 0$, precisely at the intersection points of the 1-cycles in $\Sigma_{W=0}$. Open strings at such intersections lead to the chiral bi-fundamental fields. Moreover, disks in Σ bounded by pieces of different 1-cycles lead to superpotential terms generated by world-sheet instantons.

Hence, the structure of the 3-cycles, and hence of the gauge theory, is determined by the 1-cycles in the fiber Σ over $W = 0$. This structure, which is naturally embedded in a $\mathbf{T^3}$ (from the $\mathbf{T^3}$ fibration structure of the mirror geometry), admits a natural projection to a $\mathbf{T^2}$, upon which the 1-cycles end up providing a tiling of $\mathbf{T^2}$ by a bipartite graph, which is precisely the dimer diagram of the gauge theory.

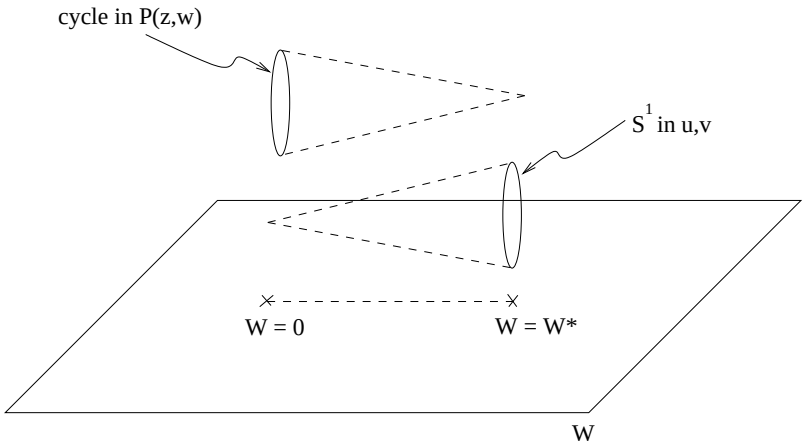

Figure 3: Structure of the non-trivial 3-cycles in the geometry $\mathcal{W}$. They are constructed by fibering over the segment joining $W = 0$ and $W = W^*$, the S^1 in the uv fiber (degenerating at $W = 0$) times the 1-cycle in the $P(z, w)$ fiber degenerating at $W = W^*$.

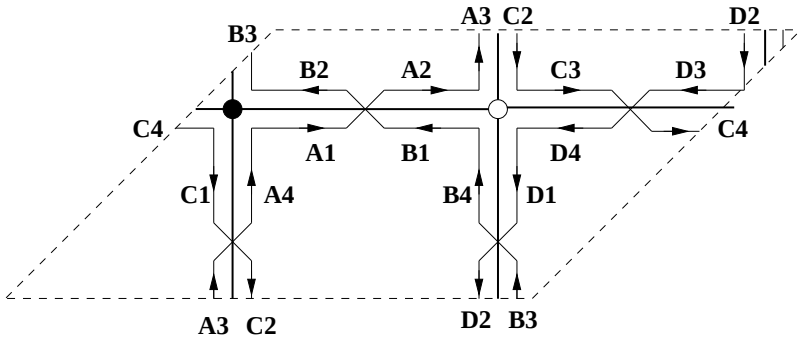

Figure 4: Dimer of the conifold with the corresponding zig-zag paths.

This last process is perhaps better understood (and of more practical use) by recovering the Riemann surface Σ from the dimer diagram of the gauge theory, as follows. Given a dimer diagram, one can define zig-zag paths (these, along with the related rhombi paths, were introduced in the mathematical literature on dimers in [43, 44], and applied to the quiver gauge theory context in [28]), as paths composed of edges, and which turn maximally to the right at e.g. black nodes and maximally to the left at white nodes. They can be conveniently shown as oriented lines that cross once at each edge and turn at each vertex, as shown in figure 4. Notice that at each edge two zig-zag paths must have opposite orientations. For dimer models describing toric gauge theories, these zig-zag paths never intersect themselves and form closed loops wrapping (p, q) cycles on the $\mathbf{T^2}$. This is shown for the conifold in figure 4 where the zig-zag paths A, B, C and D have charges (0,1), (-1,1), (1,-1), (0,-1) respectively.

As shown in [29], the zig-zag paths of the dimer diagram associated to D3-branes at a singularity lead to a tiling of the Riemann surface Σ in the mirror geometry. Specifically,

JHEP06(2006)055

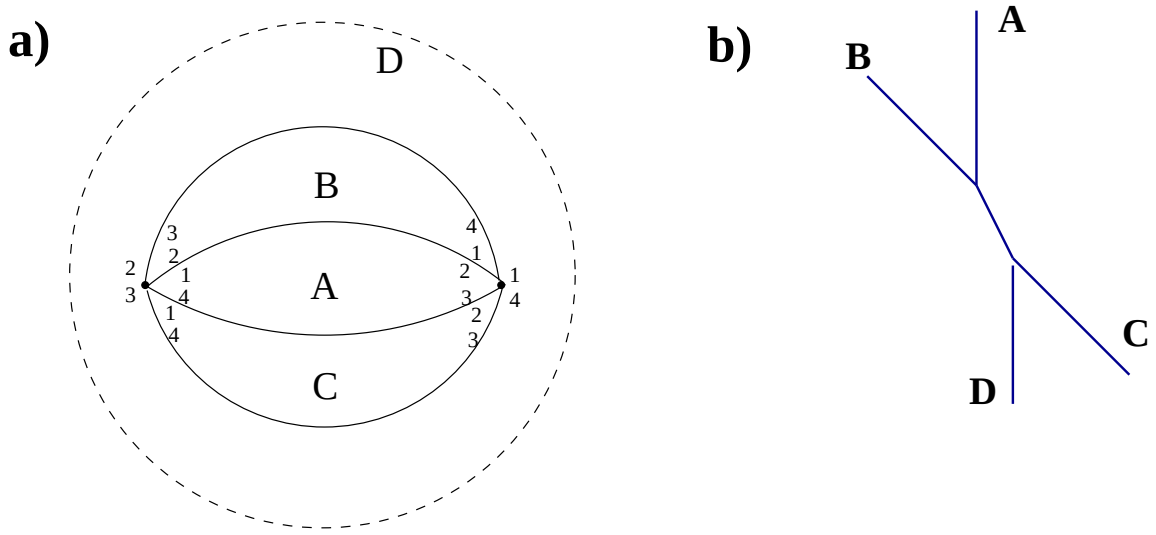

Figure 5: a) Tiling of the Riemann surface (which is topologically a sphere, shown as the complex plane) for the case of D3-branes at a conifold singularity. b) The web diagram, providing a skeleton of the Riemann surface, with asymptotic legs corresponding to punctures (and hence to faces of the tiling of Σ, and zig-zag paths of the original dimer diagram).

each zig-zag path encloses a face of the tiling of Σ which includes a puncture, and the (p, q) charge of the associated leg in the web diagram is the (p, q) homology charge of the zig-zag path in the $\mathbf{T^2}$. The touching of two of these faces in the tiling of Σ corresponds to the coincidence of the corresponding zig-zag paths along an edge of the dimer diagram. The tiling of Σ for the conifold is shown in figure 5a, while the corresponding web diagram is shown in figure 5b.

The dimer diagram moreover encodes the 1-cycles in the mirror Riemann surface, associated to the different gauge factors in the gauge theory. Consider a gauge factor associated to a face in the dimer diagram. One can consider the ordered sequence of zig-zag path pieces that appear on the interior side of the edges enclosing this face. By following these pieces in the tiling of Σ one obtains a non-trivial 1-cycle in Σ which corresponds precisely to that used to define the 3-cycle wrapped by the mirror D6-branes carrying that gauge factor. Using this map, it is possible to verify all dimer diagram rules (edges are bi-fundamentals, nodes are superpotential terms) mentioned at the beginning. An amusing feature is that these non-trivial 1-cycles in Σ are given by zig-zag paths of the tiling of Σ. The non-trivial 1-cycles in the mirror Riemann surface for the case of the conifold are shown in figure 6.

2.3 Perfect matchings

A last concept we would like to discuss is that of perfect matchings for a dimer diagram. A perfect matching is a subset of edges of the dimer diagram, such that every vertex of the graph is the endpoint of exactly one such edge. In figure 7 we show the four perfect matchings for the conifold. For future convenience, we consider the edges in each perfect matching to carry an orientation, e.g. from black to white nodes.

JHEP06(2006)055

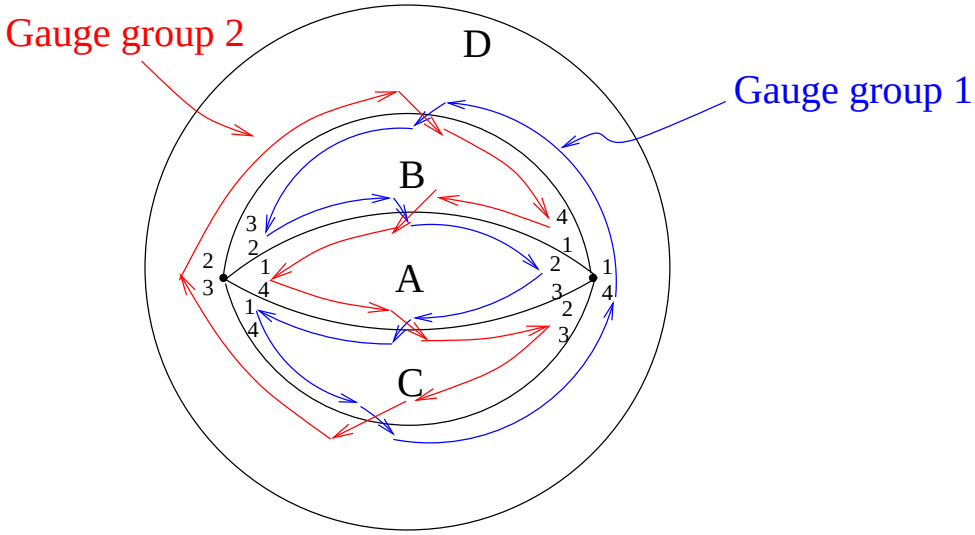

Figure 6: Tiling of the Riemann surface for the case of D3-branes at a conifold singularity, with the 1-cycles corresponding to the two gauge factors (shown as zig-zag paths of the tiling of Σ).

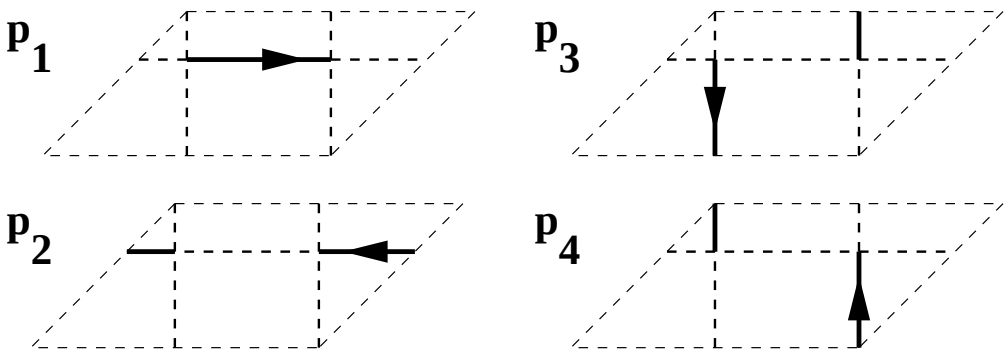

Figure 7: Perfect matchings for the dimer of the conifold.

As discussed in [27] and proved in [30], there is a one to one correspondence between the perfect matchings for a dimer diagram and the linear sigma model fields that arise in the construction of the moduli space of the quiver gauge theory [2, 7, 9]. This implies that each perfect matching has an associated location in the toric diagram of the corresponding singularity. This can be obtained as follows. Fix a given perfect matching as reference matching, denoted p_0. Then for any perfect matching p_i we can consider the path $p_i - p_0$, obtained by superimposing the edges of p_i and those of p_0, with flipped orientation for the latter. With the convention that repeated edges with opposite orientation annihilate, we obtain a (possibly trivial, or even empty) path in the dimer diagram, carrying a (possibly trivial) $\mathbf{T^2}$ homology charge (n_i, m_i). Then the location of the matching p_i in the toric diagram is given by $(-m_i, n_i)$. This definition is equivalent to that using the height functions, so we denote $(h_{x,i}, h_{y,i}) = (-m_i, n_i)$ the slope of p_i. Clearly the choice of reference matching simply amounts to a choice of origin in the toric diagram.

JHEP06(2006)055

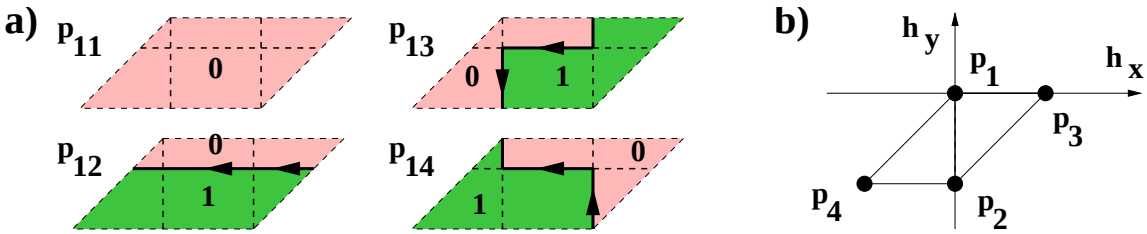

Figure 8: The paths $p_{1i} = p_i - p_1$ for the dimer of the conifold are associated to specific locations in the toric diagram, as determined by the slopes, or equivalently by the integers $(-m, n)$ where (n, m) are the homology charges of $p_i - p_1$.

For completeness, let us mention the direct definition of the slope for a perfect matching, see e.g. [27]. The dimer path $p_i - p_0$ divides the infinite tiling of $\mathbf{R^2}$ into regions that can be labeled by an integer, with the rule that each crossing of the path changes the label by one unit (up- or downwards depending on orientation of the crossing). This label assignment, when regarded in the torus, is multivalued. The holonomies around the two fundamental 1-cycles are denoted (h_x, h_y) and are called the slope of p_i.

In figure 8a we have shown the paths $p_i - p_1$ in the dimer diagram for the conifold (along with the labeling by integers to obtain the slopes). The location of the perfect matchings in the toric diagram in shown in figure 8b.

Although not emphasized in the literature, there is a beautiful interpretation of pairs of perfect matchings. From a construction similar to the above, to any pair of perfect matchings p_i, p_j one can associate a path (which we call 'difference path') $p_{ij} = p_j - p_i$ in the dimer diagram, with $\mathbf{T^2}$ homology charge $(\Delta n, \Delta m)$. In the toric diagram this is associated to the segment joining the location of p_i to that of p_j, which as a vector is given by the slope difference $(\Delta h_x, \Delta h_y) = (-\Delta m, \Delta n)$. Now clearly, the homology charge $(\Delta n, \Delta m)$ is precisely the (p, q) charge of the segment in the web diagram dual to that segment in the toric diagram. This suggests a natural interpretation of $p_j - p_i$ in the mirror Riemann surface. Indeed, by lifting the dimer path $p_j - p_i$ to the mirror Riemann surface (using the tiling of the latter) one obtains a non-trivial 1-cycle which winds around the tube corresponding to the thickening of the leg in the web diagram. This is illustrated in figure 9 for the case of the conifold.

Clearly, the dimer paths associated to adjacent external matchings (i.e. matchings which are at adjacent locations on the boundary of the toric diagram) carry the same charges as zig-zag paths (although in general may not coincide edge by edge with them). This hence shows the equivalence of the two ways we have described to obtain the toric diagram associated to a dimer diagram[6] (namely, construction of the web diagram by using charges of zig-zag paths, and construction of the toric diagram using height functions).

[6]Yet another equivalent way, not used in this paper, is the computation of the determinant of the Kasteleyn matrix, see e.g. [26, 27].

JHEP06(2006)055

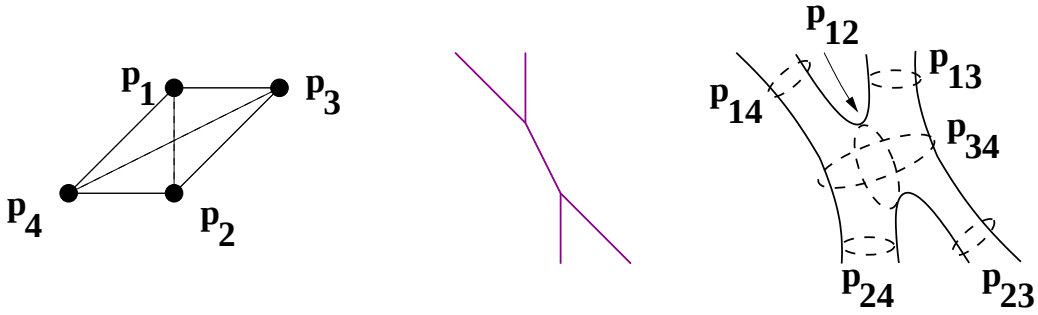

Figure 9: The perfect matchings for the dimer of the conifold are associated to specific locations in the toric diagram, as determined by the slopes. The paths $p_{ij} = p_i - p_j$ correspond to 1-cycles in the mirror Riemann surface wrapped around the tubes dual to the segment joining p_i and p_j in the toric diagram.

3. Partial resolution

In this section we provide a description of the effect of general partial resolutions on the gauge theory using dimer diagram techniques. The simplest class of partial resolutions corresponds to the removal of a triangle in the toric diagram. There are however more involved possibilities, like the splitting of a singularity into two singularities (examples will come later). Clearly, the former can be regarded as a particular case of the latter, with the second 'singularity' being a smooth patch of the final geometry.

Minimal partial resolutions (those removing one triangle of the toric diagram) and their relation to the D3-brane gauge theory (appearance of a Fayet-Iliopoulos term triggering a Higgs mechanism) were discussed in [7]. This process was described as removal of edges in the dimer diagram in [27]. However, in both cases the mapping between a particular operation on the gauge theory/dimer diagram and the resulting geometry, was manifest only upon computation of the moduli space of the gauge theory. This makes it difficult to obtain the gauge theory corresponding to a given partial resolution, and requires some trial and error. Also, the description of more involved partial resolutions (splitting the singularities) and their gauge theory/dimer diagram counterpart was not provided. Moreover, as pointed out and explained in [28], arbitrary addition/removal of edges in a dimer diagram can lead to inconsistent theories.

In this section we consider an arbitrary partial resolution of a toric singularity, typically splitting it into several. We consider the original set of D3-branes to split accordingly into subsets located at the daughter singular points. Hence one expects that the original gauge theory splits (via a Higgs mechanism) into several gauge sectors, decoupled at the level of massless modes, and correspondingly that the original dimer diagram splits into several sub-dimers associated to the subsets of D3-branes at the daughter singularities. We provide a simple construction of the splitting of dimer diagrams that corresponds to a given partial resolution. In addition, we provide a simple recipe for the bi-fundamental vevs that trigger the corresponding Higgsing in the gauge theory.

As a prototypical example we consider partial resolutions splitting a singularity into two. Other cases, like minimal partial resolutions, can be recovered as a particular case

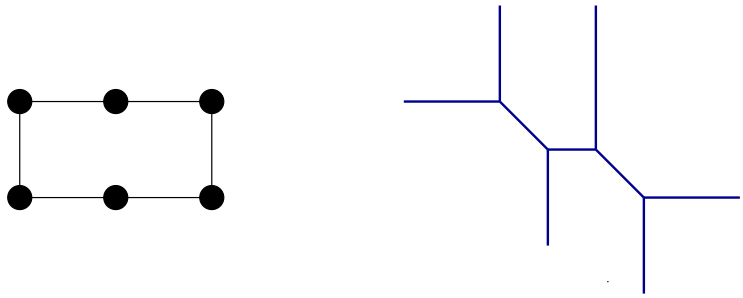

Figure 10: The toric diagram and web diagram of the double conifold singularity $xy = s^2w^2$. For clarity, we show the web diagram for a slightly resolved geometry.

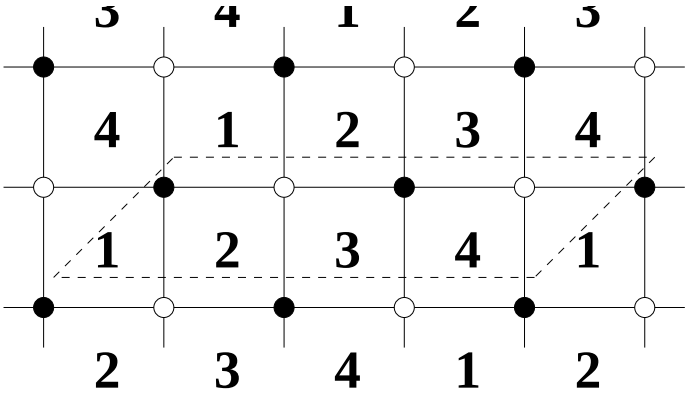

Figure 11: Dimer diagram corresponding to the double conifold singularity in figure 10. The dashed line corresponds to the unit cell of the periodic tiling.

as mentioned above. Splitting into more than two daughter singularities can be easily obtained by iteration of our procedure.

3.1 An example in detail

Let us start with a simple example of the splitting via partial resolution of a singularity into two singularities, using concepts and techniques from dimers.

Consider the singularity whose toric diagram and web diagram are shown in figure 10. This singularity, and the gauge theory on D3-branes located on it, have been studied in [49, 48]. We refer to it as the double conifold. The dimer diagram shown in figure 11 provides (a toric phase of) the gauge theory on D3-branes at this double conifold singularity.

The above singularity admits partial resolutions to geometries with two separated singularities. One such partial resolution is illustrated in figure 12a, and corresponds to a large blow up of an $\mathbf{S^2}$, smoothing the initial geometry to two isolated conifold singularities. A different splitting, into two $\mathbf{C^2/Z_2}$ (times $\mathbf{C}$) singularities, is shown in figure 12b.

The partial resolution corresponds to turning on Fayet-Iliopoulos terms in the D3-brane gauge theory.[7] These FI terms force some of the bi-fundamental scalars to acquire a vev,

[7] This is if the U(1) factors are included in the gauge theory. In fact, these U(1) factors are generically

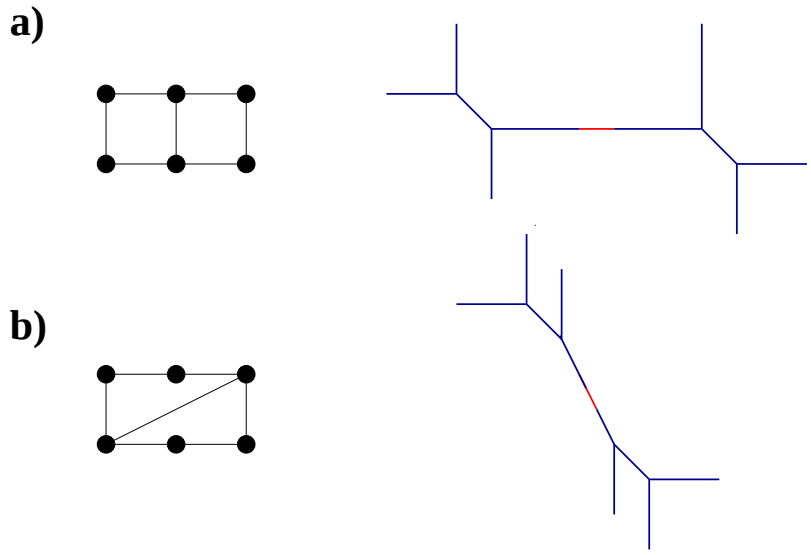

Figure 12: Partial resolution of the double conifold singularity in figure 10, splitting the initial singularity into (a) two isolated conifold singularities; (b) two $\mathbf{C^2/Z_2}$ (times $\mathbf{C}$) singularities. The distance between the daughter singularities is controlled by the size of the $\mathbf{S^2}$ corresponding to the dashed red segment in the associated web diagram. For clarity the web diagrams of the left-over singularities are shown for slightly resolved geometries.

breaking the gauge symmetry. For the case of a partial resolution splitting a singularity, the left over field theory must correspond to two gauge sectors, corresponding to the gauge theories on stacks of D3-branes at the two singularities. These two sectors are decoupled at the level of massless states. Namely, the only states charged under both sectors are massive, with mass controlled by the bi-fundamental vevs, and hence to the size of the 2-sphere responsible for the splitting. This agrees with the picture of open strings stretching between the two stacks of D3-branes. In section 3.3 we will be more explicit about the precise set of vevs corresponding to splitting singularities.

In this section, our aim is to provide a simple recipe that implements the effect of the resolution on the gauge field theory. This will be expressed in terms of a simple operation that, starting from the dimer of the initial singularity, leads to two sub-dimers corresponding to the gauge theories in the two daughter singularities.

The geometrical effect of partial resolutions is most manifest in the web diagram. Let us for concreteness consider the partial resolution of the double conifold to two conifolds, figure 12a. As described in section 2.2 the web diagram is encoded in the dimer diagram via its structure of zig-zag paths [28, 29]. The zig-zag paths corresponding to the dimer in figure 11 are shown in figure 13. The corresponding asymptotic legs in the web diagram, and the tiling of the mirror Riemann surface Σ, are shown in figure 14.

massive, hence disappear from the low energy effective theory. In this viewpoint, the partial resolution corresponds to vevs for suitable baryonic operators. We however find it more convenient to include the U(1)'s explicitly, and consider the couplings rendering them massive at a subsequent stage. See [50, 7] for a more detailed discussion.

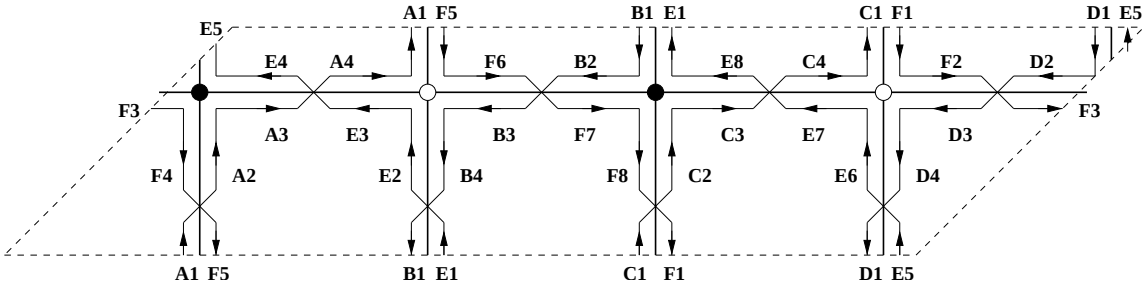

Figure 13: Zig-zag paths for the dimer diagram of the double conifold.

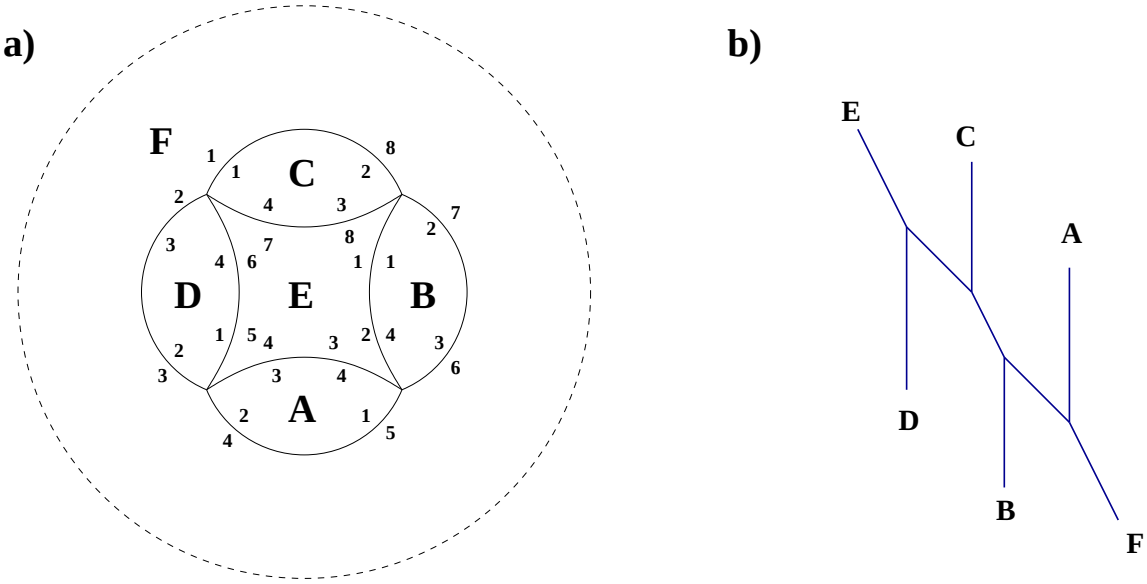

Figure 14: (a) Zig-zag paths in figure 13 correspond to external legs in the web diagram of the singularity. (b) The adjacency relations among zig-zag paths encode a tiling of the mirror Riemann surface Σ, which in this case corresponds to a 2-sphere with six punctures, realized in the picture as the complex plane (with the point at infinity).

In this language, it is easy to realize that the partial resolution corresponds to factorizing the Riemann surface Σ by an elongated tube, as in figure 15a. The structure of the two left over singularities can be determined by analyzing the local structure of the two daughter Riemann surfaces. Due to the factorization along the infinite tube, each daughter Riemann surface has a new puncture, denoted G, which must correspond to a new zig-zag path in the corresponding daughter dimer diagram. In particular, the decomposition of the tiling of Σ upon this factorization, shown in figure 15b, leads to two sets of zig-zag paths, namely C, D, E, G and A, B, F, G, respectively, with specific adjacency relations. This information can be used to construct two dimer diagrams, which encode the gauge theories on D3-branes at the two singular points in the geometry after partial resolution.

In figure 16 we show the two sets of zig-zag paths. For convenience, the inherited paths are drawn in the locations corresponding to the original dimer. The information from the

JHEP06(2006)055

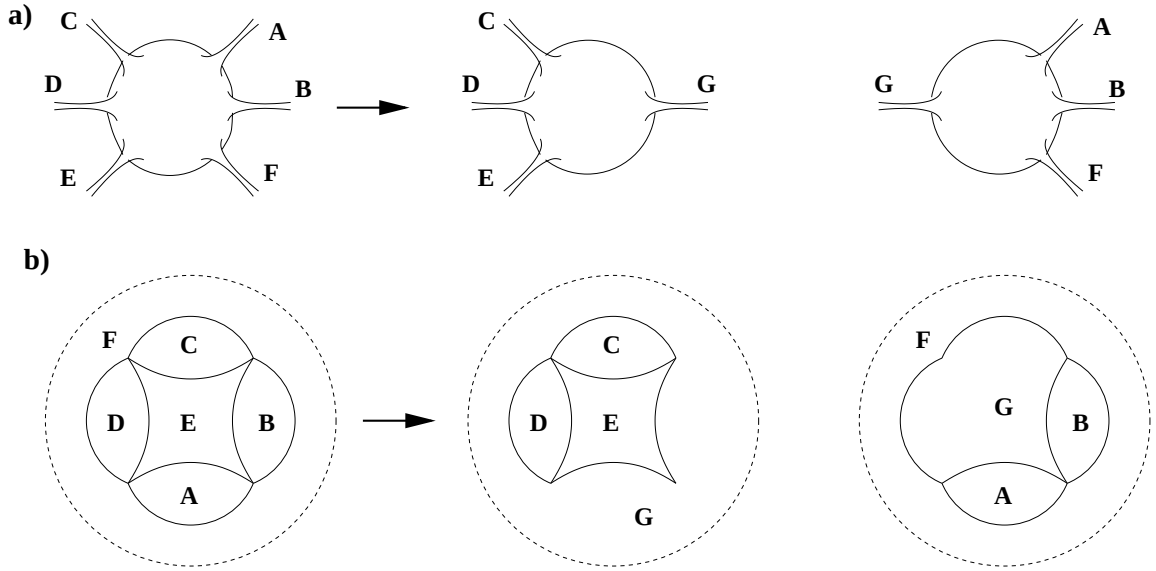

Figure 15: (a) Schematic representation of the factorization of the mirror Riemann surface Σ. (b) Decomposition of the tiling of Σ upon factorization. The two new sets of zig-zag paths, and their adjacency relations, can be used to construct the two dimers corresponding to D3-branes at the two singularities after splitting of the geometry.

zig-zag paths allows to construct the dimer diagram corresponding to D3-brane at each of the left-over singularities after partial resolution. The dimer diagrams are also shown in the picture.

It is easy to convince oneself that the two theories are isomorphic (as expected from the symmetric factorization of the Riemann surface, or of the web diagram). Hence, it is enough to focus in one of them, say that shown in figure 17a. Since this theory has a bi-valent node, one should integrate out the corresponding massive matter, with the result shown in figure 17b. This can be redrawn as in figure 17c, and one recognizes the dimer diagram for the conifold singularity, as expected. Hence the above technique of zig-zag paths provides a simple tool to determine the effect of a splitting by partial resolution on the dimer diagram of the D3-brane gauge theory, as a specific splitting of the initial dimer into two sub-dimers. Moreover, in section 3.3 we will show that the operation in the dimer diagram encodes in a simple manner the set of bi-fundamental vevs that corresponds in the gauge field theory to the partial resolution of the singularity.

The whole procedure can be subsumed in a simple operation in the dimer diagram, without the need to go through the Riemann surface. In terms of the dimer diagram the previous discussion amounts to drawing the old zig-zag paths that define the remaining singularity we are interested in (C, D and E in the example above), and then completing with new zig-zag paths (this will be G) until all edges have two zig-zag paths going through them. The number of required new paths is given by the decrease in the number of holes in the factorization plus one. In the remaining examples we will obtain our results by using this simple shortcut.

JHEP06(2006)055

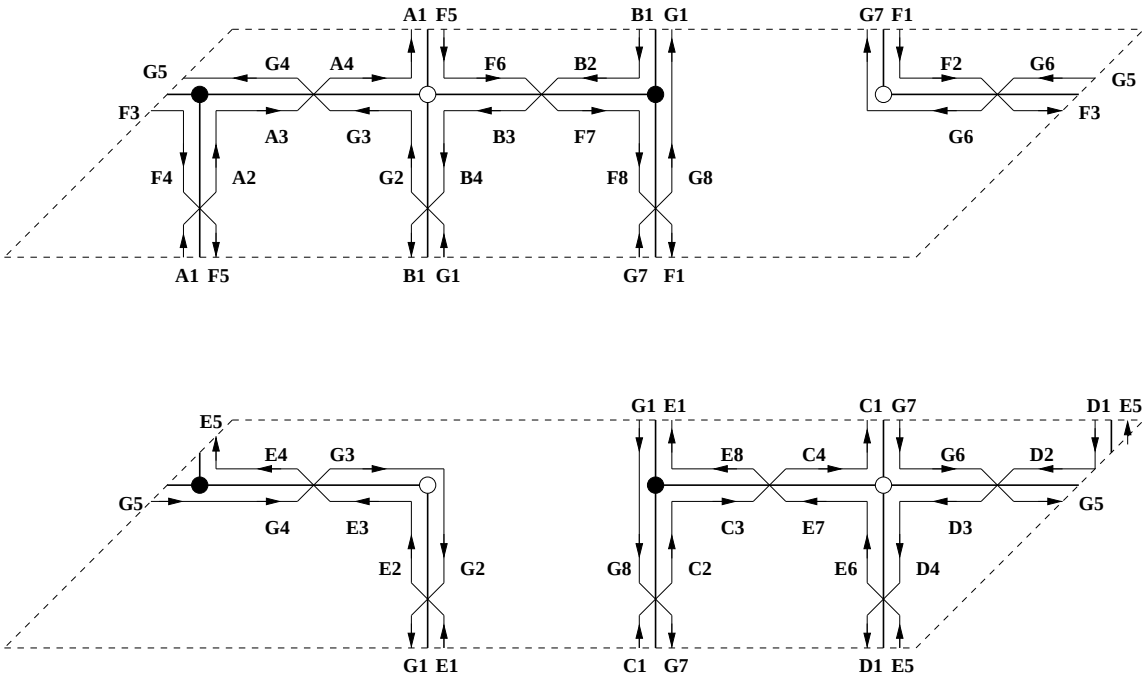

Figure 16: Zig-zag paths corresponding to the two daughter theories, in the splitting of the double conifold singularity to two conifold singularities, with the corresponding dimers shown as thick lines.

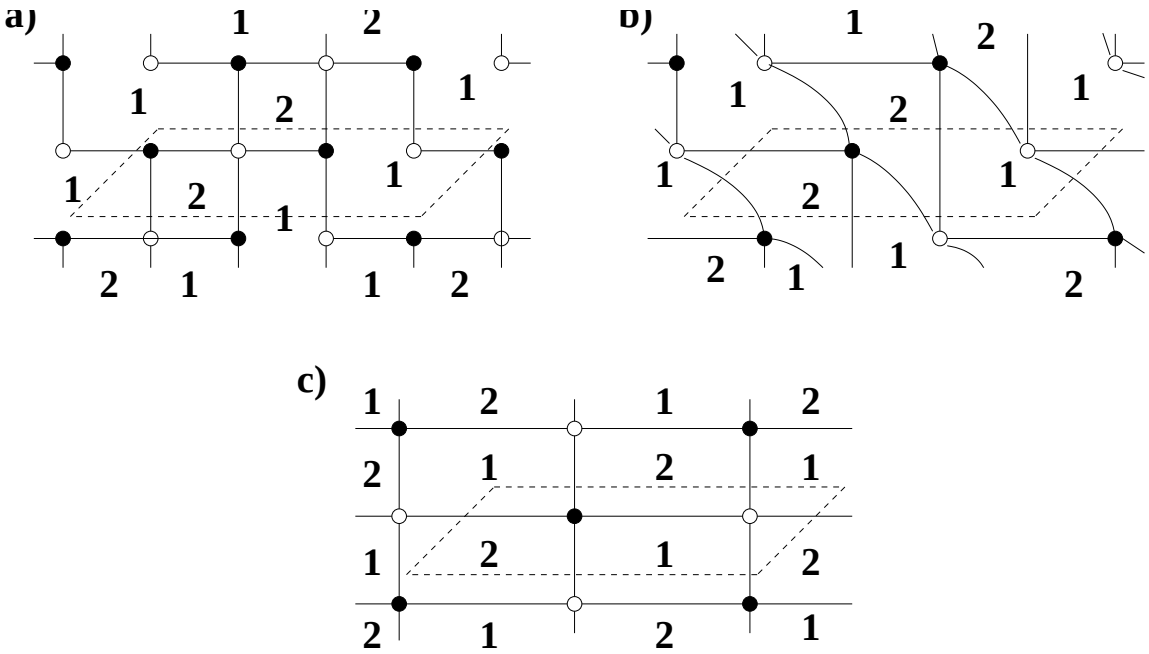

Figure 17: (a) Dimer diagram corresponding to the first picture in figure 16. Figure (b) shows the dimer of the theory after integrating out massive modes. An equivalent diagram is shown in figure (c), where one recognizes the dimer diagram of the conifold theory.

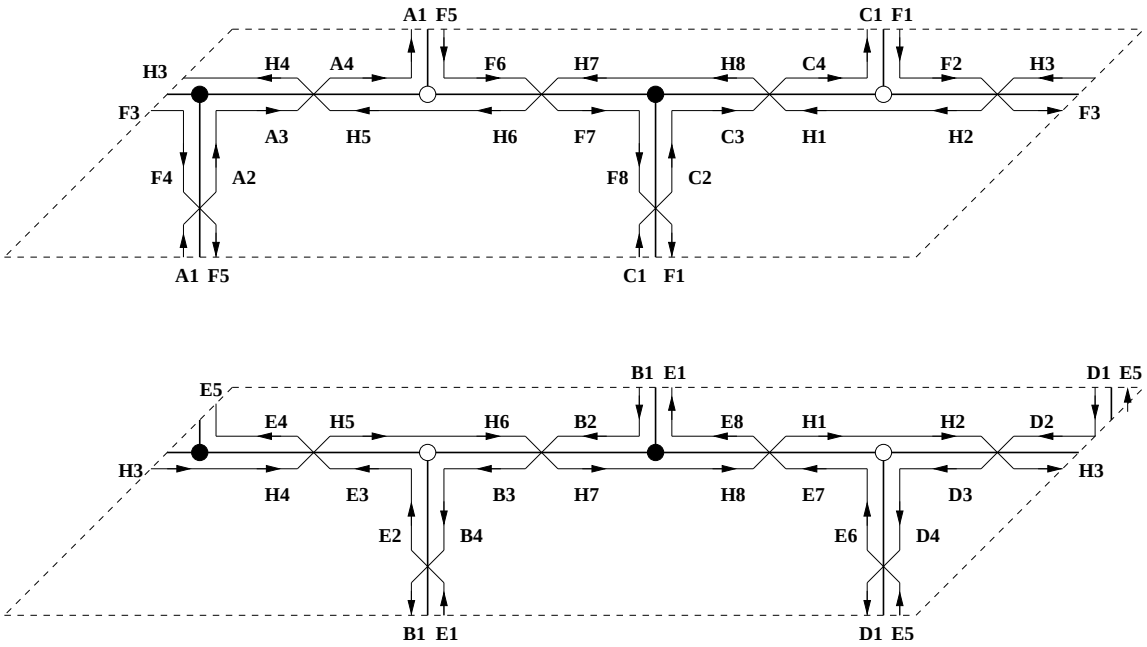

Figure 18: Zig-zag paths corresponding to the two daughter theories, in the splitting of the double conifold singularity to two $\mathbf{C^2/Z_2}$ singularities, with the corresponding dimers shown as thick lines.

3.2 Further examples and comments

3.2.1 Double conifold to two $\mathbf{C^2/Z_2}$ singularities

The technique we have described in the above example is fully general, and can be applied to any partial resolution. To provide an additional example, consider for instance the splitting of the above singularity into two $\mathbf{C^2/Z_2}$ singularities, figure 12b. Starting with the zig-zag paths in figure 13, the partial resolution corresponds to a factorization of the mirror Riemann surface splitting the set of paths into two subsets, namely A, C, F, and B, D, E. Each set, along with a new path H from the new puncture in the daughter Riemann surface, allow to read off the dimer diagrams (and hence the quiver gauge theories) for D3-branes in the two left-over singularities. This is shown in figure 18, where one indeed recognizes the dimer diagrams of two $\mathbf{C^2/Z_2}$ theories.

3.2.2 From dP_3 to two SPP's

Before concluding this section, we present a further example, where the factorization lowers the genus of the mirror Riemann surfaces. Namely, the factorization implies elongating several segments in the web diagram. Consider for instance the splitting of the complex cone over dP_3 to two suspended pinch point (SPP) singularities, shown in figure 19.

The dimer diagram for (a toric phase of) the gauge theory on D3-branes at the cone over dP_3 is shown in figure 20. The unit cell of the corresponding dimer diagram is shown in figure 21, where we also show the zig-zag paths. The partial resolution in figure 19 has the effect of splitting this dimer diagram into the two dimer diagrams in figure 22.

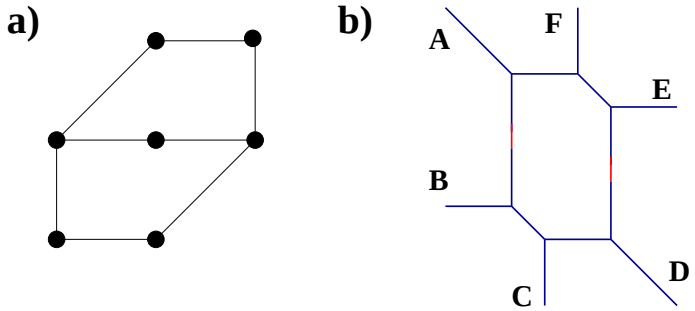

Figure 19: The toric diagram and web diagram of the complex cone over dP_3, in a splitting to two SPP singularities. For clarity, the web diagrams of the left-over SPP singularities are shown for slightly resolved geometries. For future convenience, we have labeled external legs.

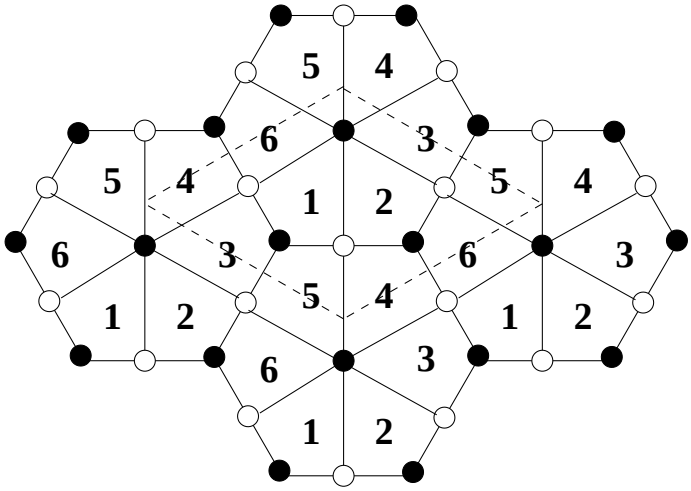

Figure 20: The dimer diagram for the gauge theory of D3-branes on the complex cone over dP_3.

After integrating out massive fields, they can be shown to correspond to the gauge theories of D3-branes at SPP singularities, in agreement with the underlying geometric picture. Although this example follows from exactly the same rules as previous ones, we encounter the new feature that the splitting of the dimer involves two new zig-zag paths (denoted G and H) rather than one. This simply reflects the fact that the factorization of the Riemann surface involves two elongated tubes, hence two new punctures for each daughter Riemann surface.

3.2.3 Minimal partial resolution

To conclude this section, we would like to mention that this technique can be applied to asymmetric splittings, where the two daughter geometries are not the same. One particular extremal case is a minimal partial resolution (removing only one triangle from the toric diagram). Hence, only one singularity is left over after the partial resolution (namely the second singularity turns out to be a smooth patch). Let us describe this more explicitly.

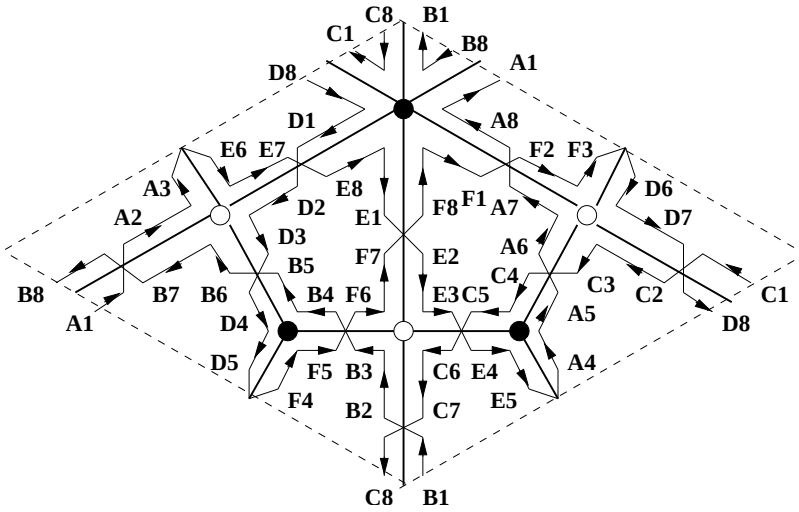

Figure 21: The figure shows the unit cell of the dimer diagram for the gauge theory of D3-branes on the complex cone over dP_3, and the set of zig-zag paths.

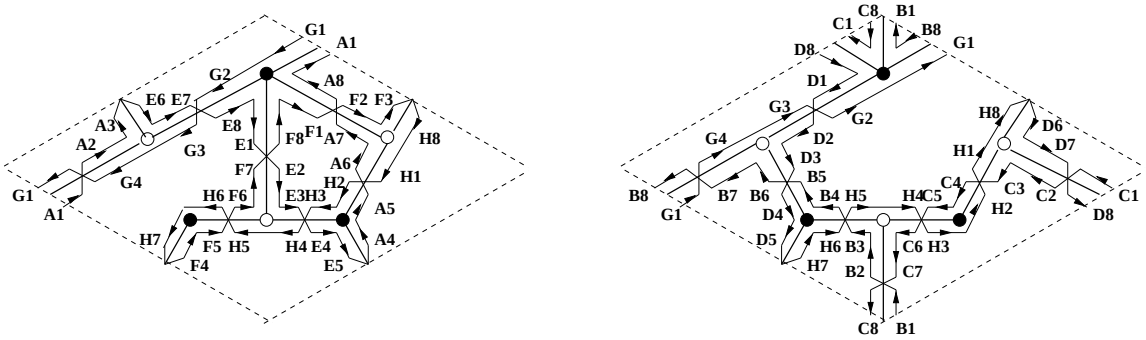

Figure 22: The two dimers obtained upon the splitting by small resolution shown in figure 19. They can be shown to be equivalent to two copies of the SPP dimer diagram.

In terms of the web diagram, this simply corresponds to elongating a tube that separates two external legs from the rest of the web. Using the zig-zag paths, it is easy to show that the left-over singularity corresponds to a dimer diagram obtained from the initial one by the removal of some edges. These edges are precisely those over which the two zig-zag paths associated to the removed legs overlap[8]

To provide one particular example, we describe the partial resolution of the double conifold to an SPP singularity via the removal of one triangle in the corresponding toric diagram. Concretely consider separating the legs A and F from the rest of the web diagram, by stretching the intermediate segment. Since the corresponding zig-zag paths overlap over

[8]This description explains as in [28] the possibility of the appearance of inconsistent dimer diagrams by arbitrary addition/removal of edges. For instance, consider a minimal partial resolution involving two zig-zag paths overlapping over more than one edge. The removal on only one of these edges does not correspond to a consistent separation of zig-zag paths and leads to an inconsistent diagram.

JHEP06(2006)055

the lower left edge in the dimer diagram, this is the edge to be removed. In field theoretic terms this means that the corresponding bifundamental gets a vev, and the two faces (gauge groups) sharing the edge join (gauge factors break to the diagonal combination). The resulting dimer diagram is that of the SPP theory, as can be checked by computing the gauge theory data.

We hope these examples suffice to illustrate the general validity of the above prescription.

3.3 Field theory interpretation

As discussed in [7], partial resolutions of singularities correspond to turning on Fayet-Iliopoulos terms on the gauge theory on D3-branes sitting at them. These FI terms force some of the bi-fundamental scalars to acquire vevs, preserving supersymmetry but partially breaking gauge symmetry, in precise agreement with the quiver gauge theory on D3-branes at the final left-over singularity.

In this section we show that the operation of splitting a dimer, as described in previous section, encodes in a very precise fashion the field theory data corresponding to the Higgs mechanism and gauge symmetry breaking. Moreover we show that dimer techniques can be efficiently used to show the F- and D-flatness of such vevs.

For simplicity, we center on a gauge theory with all gauge factors having equal rank N. Discussion of other situations (fractional branes) is postponed until section 3.5. We also consider that after the splitting, N_1 D3-branes remain at the first singularity and N_2 remain at the second.

In order to describe the bi-fundamental vevs in the field theory, we notice that in the dimer splitting there are three different kinds of bi-fundamental fields, according to the behaviour of the corresponding edge: a) those appearing in the two daughter dimers; b) those not appearing in the first sub-dimer, but present in the second; c) those not appearing in the second, but present in the first. This suggests the following ansatz for their vevs, which we denote V_0, V_1, V_2, respectively:

$$V_0 = \begin{pmatrix} 0 & 0 \\ 0 & 0 \end{pmatrix}; \qquad V_1 = \begin{pmatrix} v\,\mathbf{1}_{N_1} & 0 \\ 0 & 0 \end{pmatrix}; \qquad V_2 = \begin{pmatrix} 0 & 0 \\ 0 & v\,\mathbf{1}_{N_2} \end{pmatrix} \tag{3.1}$$

where bi-fundamental fields are regarded as $N \times N$ matrices, and the entries are blocks of dimension appropriate to the partition $N = N_1 + N_2$. Here we take v to be adimensional, and we consider that a dimensionful constant enters into the vev of each bi-fundamental, exponentiated to the appropriate power to match its conformal dimension. This factor does not change the discussion of flatness, hence we ignore it in what follows.

The interpretation of this ansatz is very clear. The N_1, N_2 entries in the diagonal determine the pattern of gauge symmetry breaking triggered by that bi-fundamental for the set of the N_1, N_2 D3-branes in the first, resp. second dimer. An edge absent in a sub-dimer implies a local recombination of the corresponding set of D3-branes across the associated bi-fundamental. Namely, there is a non-vanishing vev in the corresponding set of entries. Similarly, for edges present in a sub-dimer there is no vev in the corresponding entries of the associated bi-fundamentals.

JHEP06(2006)055

The proof that the above assignment of vevs satisfies the flatness conditions in the field theory is provided in appendix A. However it is useful to work out an explicit example, so consider for instance the splitting of the double conifold to two conifold singularities. Using the information in figure 11 for the initial dimer, and figure 16 for the sub-dimers, we obtain the following set of vevs

$$\begin{aligned} &\Phi_{12} = V_2\,, \qquad \Phi_{23} = V_2\,, \qquad \Phi_{34} = V_0\,, \qquad \Phi_{41} = V_0 \\ &\Phi_{21} = V_0\,, \qquad \Phi_{32} = V_0\,, \qquad \Phi_{43} = V_1\,, \qquad \Phi_{14} = V_1 \end{aligned} \tag{3.2}$$

where we have introduced the notation Φ_{ij} for a bi-fundamental $(\square_i, \overline{\square}_j)$, and take Φ_{12} to correspond to the vertical edge in the left part of the depicted unit cell.

It is now straightforward to analyze the flatness conditions on the set of vevs for this example. Concerning the F-term conditions, all nodes are 4-valent, hence the superpotential is a sum of quartic terms. Moreover, any such term contains at least two fields without vev. Hence, the F-terms conditions are automatically satisfied. Concerning the non-abelian D-term conditions, we write the generators of SU(N) as

$$T = \begin{pmatrix} T_{11} & T_{12} \\ T_{21} & T_{22} \end{pmatrix} \tag{3.3}$$

and obtain that the D-term contributions for the SU$(N)_i$ factors are

$$\begin{aligned} \mathrm{SU}(N)_1 \qquad & \mathrm{tr}\,(\Phi_{12}^\dagger T \Phi_{12}) + \mathrm{tr}\,(\Phi_{14}^\dagger T \Phi_{14}) = |v|^2(\mathrm{tr}\,T_{11} + \mathrm{tr}\,T_{22}) = 0 \\ \mathrm{SU}(N)_2 \qquad & -\mathrm{tr}\,(\Phi_{12}^\dagger T \Phi_{12}) + \mathrm{tr}\,(\Phi_{23}^\dagger T \Phi_{23}) = |v|^2(\mathrm{tr}\,T_{22} - \mathrm{tr}\,T_{22}) = 0 \\ \mathrm{SU}(N)_3 \qquad & -\mathrm{tr}\,(\Phi_{23}^\dagger T \Phi_{23}) - \mathrm{tr}\,(\Phi_{43}^\dagger T \Phi_{43}) = -|v|^2(\mathrm{tr}\,T_{11} + \mathrm{tr}\,T_{22}) = 0 \\ \mathrm{SU}(N)_4 \qquad & \mathrm{tr}\,(\Phi_{43}^\dagger T \Phi_{43}) - \mathrm{tr}\,(\Phi_{14}^\dagger T \Phi_{14}) = |v|^2(\mathrm{tr}\,T_{11} - \mathrm{tr}\,T_{11}) = 0 \end{aligned} \tag{3.4}$$

where we have used tracelessness of SU(N) generators. Finally, concerning the abelian D-term conditions, the above vevs lead to non-zero contributions which are suitably canceled by the non-zero FI terms. This effective absence of U(1) D-term constraints can be equivalently regarded as the statement that there are $B \wedge F$ couplings (related to the FI terms by supersymmetry) which render the U(1)'s massive, so that they are not present at low energies and hence no D-term constraints have to be imposed, see footnote 7.

Notice that the description in this section generalizes in a straightforward fashion to the splitting of a dimer into more than two sub-dimers.

3.4 Effect on perfect matchings

It is interesting to consider the effect of partial resolution on perfect matchings. This can be easily analyzed at the level of the dimer diagrams, as we do in what follows in a particular example. Consider the double conifold, whose dimer diagram is shown in figure 11. The eight perfect matchings for this diagram are shown in figure 23. The location of these matchings in the toric diagram, obtained as described in section 2.3, using p_1 as reference matching, are shown in figure 24a.

Consider the partial resolution of the double conifold to two conifolds, studied in section 3.1, whose two resulting sub-dimers are shown in figure 16. The splitting of the

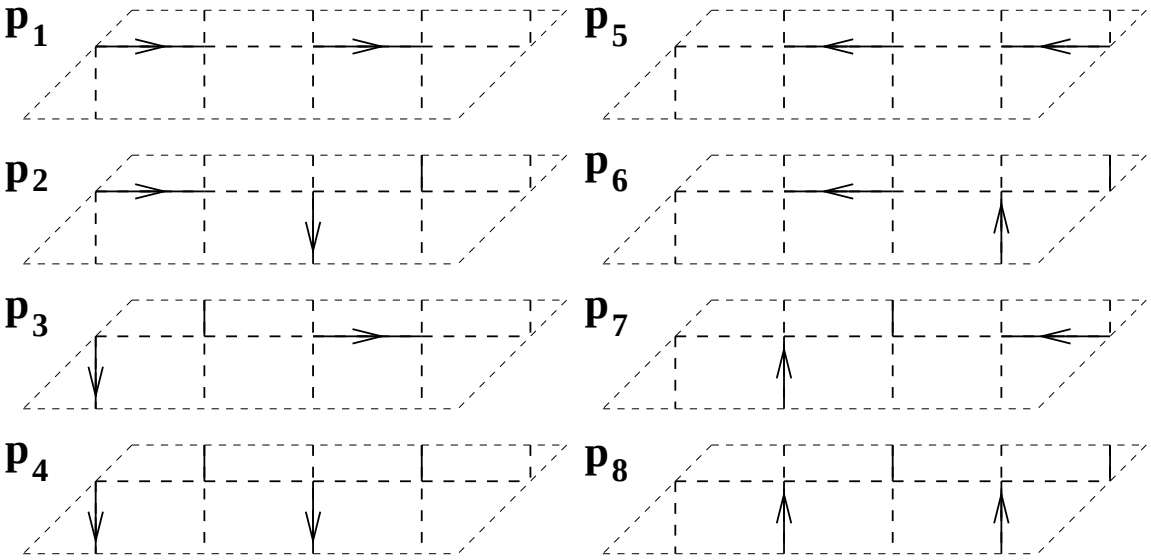

Figure 23: The eight perfect matchings for the dimer diagram of the double conifold.

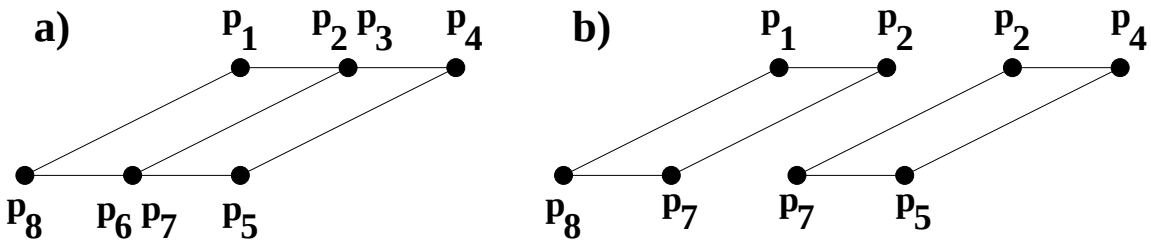

Figure 24: In a partial resolution, the original perfect matchings descending to perfect matchings of one or the other subdimer end up located at one or the other toric sub-diagram, as shown here for the resolution of the double conifold to two conifolds.

dimer into sub-dimers implies that the perfect matchings of the original dimer fall into different classes:

- The perfect matchings p_4, p_5 descend to perfect matchings of the first sub-dimer.
- The perfect matchings p_1, p_8 descend to perfect matchings of the second sub-dimer.
- The perfect matchings p_2, p_7 correspond to perfect matchings of both the first and second sub-dimer.
- The perfect matchings p_3, p_6 do not correspond to perfect matchings of either sub-dimer.

This correspondence becomes nicely meaningful when one considers the location of the different perfect matchings in the toric diagram. The partial resolution splits the toric diagram in two pieces, separated by a common internal segment. Perfect matchings of the original dimer which descend to perfect matchings of a given sub-dimer are located at points

on the piece of the toric diagram describing the corresponding daughter singularity. Perfect matchings descending to matchings of both singularities are located along the common segment in the toric diagram. This is described for the double conifold in figure 24.

It is possible to show that this pattern is completely general, and that for a general partial resolution perfect matchings fall into one of these four classes. Namely, we label the edges of the dimer diagram with labels 1, 2 and 3, according to whether it is present in sub-dimer one, or in sub-dimer 2, or in both. Perfect matchings involving edges of type 1 and 3 end up in the interior of the toric sub-diagram 1; perfect matchings involving edges of type 2 and 3 end up in the interior of the toric sub-diagram 2; perfect matchings only involving edges of type 3 appear on both toric sub-diagrams, along their common boundary; perfect matchings with edges of type 1 and 2 (and possibly 3) disappear.

One can also obtain the effect of the partial resolution on the perfect matchings from the viewpoint of the Riemann surface. For that, one can use the relation described in section 2.3 between pairs of perfect matchings and 1-cycles on the mirror Riemann surface. The first observation is that a partial resolution corresponds to the introduction of a segment joining two external non-adjacent perfect matchings p, p' in the toric diagram. This is just dual to separating the web diagram by elongating the leg dual to that segment. Notice that cases where there are multiple matchings at the corresponding points in the toric diagram simply correspond to cases where there are several parallel legs in the web diagram, and correspondingly several possibilities to perform the partial resolution. For instance, in our above example, the partial resolution corresponds to choosing the perfect matchings p_2 and p_7.

To such a pair of perfect matchings one can associate a path $p' - p$ in the dimer diagram and a 1-cycle in the mirror Riemann surface. In fact, this 1-cycle wraps around the tube which becomes infinitely elongated in the partial resolution process. In terms of the dimer diagram, it means that the path in the dimer diagram becomes the new zig-zag path (denoted G in our example in section 3.1) introduced to construct the new sub-dimers.

Given that this 1-cycle separates the Riemann surfaces in two pieces, which are naturally associated to the two daughter singularities, it is possible to interpret the four classes of perfect matchings in terms of their behaviour on the Riemann surface Σ. Consider one of the external perfect matchings e.g. p. For any other matching p_i one can consider the 1-cycles associated to $p_i - p$ obtained using the tiling of Σ. If the whole of such 1-cycle lies on one component of Σ, the matching p_i will correspond to a perfect matching of the corresponding sub-dimer, and to a point in the corresponding toric sub-diagram. If all pieces of the 1-cycle are included in the 1-cycle $p' - p$, then p_i will correspond to a perfect matching of both sub-dimers, and will appear in both toric diagrams (concretely, along the common boundary). Finally if the 1-cycle contains pieces lying in both components of Σ, the corresponding perfect matching disappears in the process of partial resolution.

These properties are easily explicitly checked in our above example, and can be generalized to any partial resolution. We leave the discussion as an exercise for the interested reader.

JHEP06(2006)055

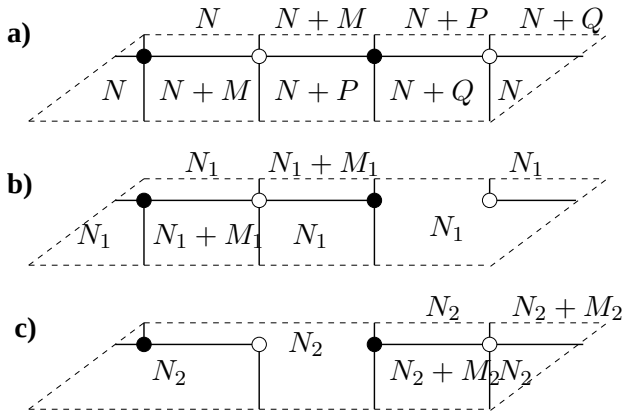

Figure 25: a) The dimer for the double conifold with the most general set of fractional branes. b,c) The sub-dimers for the daughter conifold singularities, with their fractional branes.

3.5 Partial resolutions with fractional branes

In this section we would like to study partial resolutions for singularities in the presence of fractional branes, and their description using dimers. For concreteness we center on a particular example, although our conclusions are of general validity.

Let us consider the splitting of the double conifold to two conifold singularities. The dimer diagram for the double conifold, with the most general set of fractional branes, is shown in figure 25a. Since the field theory is non-chiral, there are no restrictions on the gauge factor ranks, and hence there are three kinds of fractional branes.

When the singularity is split into two conifolds, the latter may contain fractional branes as well. The most general possibility is shown in figure 25b, c. Since each conifold allows for one kind of fractional brane, there are two possible fractional branes in the final system.

It is thus a natural question to ask what happens with the third kind of fractional brane. The answer, that we can recover from different viewpoints, is that it obstructs the partial resolution. A pictorial way to derive this result is to compare the original dimer and the daughter sub-dimers in figures 25a and b,c, respectively. In order to have a proper splitting, the number of branes in a given face of the original dimer must agree with the sum of the numbers of branes in the corresponding location in the sub-dimers. In our particular case, this implies

$$N = N_1 + N_2\,, \qquad M = M_1\,, \qquad P = 0\,, \qquad Q = M_2 \tag{3.5}$$

Hence we see that the splitting necessarily forces the fractional brane changing the rank of the gauge group 3 to be absent, in the sense that only in the absence of such brane the splitting is possible. More precisely, what obstructs the splitting is the fractional brane which controls the difference between the ranks of the gauge factors 1 and 3.

In what follows we present several interpretations for this fact. From the viewpoint of the field theory of the initial singularity, it means that the theory with different ranks for the factors 1 and 3 does not have the corresponding flat direction. This can be argued in

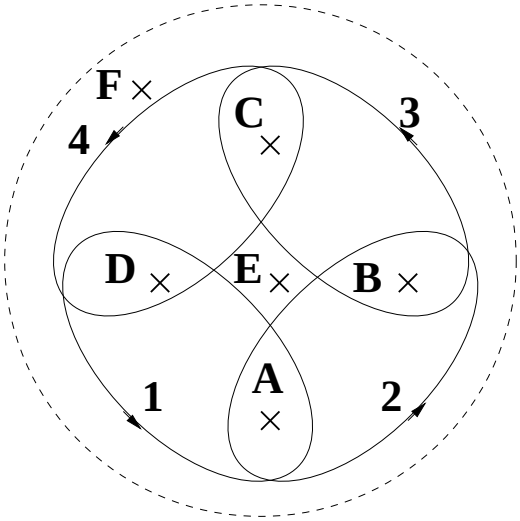

Figure 26: The 1-cycles in Σ corresponding to the D-branes controlling the rank of the different gauge factors in the double conifold gauge theory.

general, but is suffices to discuss one particular example, for instance $M = Q = 0$, $P \neq 0$. It is simple to show that the D-term conditions for gauge factor 3 cannot be satisfied. Indeed, the natural ansatz is similar to (3.2), with the only difference that for non-square matrices, the entries in the $M \times P$ additional submatrix are taken to be zero. In computing the D-term, as in (3.4), for the gauge factor 3, one notices that the non-zero vevs do not suffice to complete the full $\mathrm{SU}(M+P)$ trace, and hence the D-term does not vanish.

One can regard the dimer as realizing a physical construction of the gauge theory in terms of NS-branes and D5-branes [27], similar to brane box [45 – 47] or brane diamond models [48]. In that context, the relation between obstructions to splitting the brane configuration and D-terms in the gauge theory is familiar and well-known. Intuitively, the motion of the NS-branes drags a subset of the D5-branes, increasing their tension and breaking supersymmetry (equivalently, misaligning the phase of their BPS charge with respect to the others). In the absence of fractional branes, D5-branes on opposite sides of the NS-brane can recombine and snap back, restoring supersymmetry at the price of breaking gauge symmetry (equivalently, forming a bound state with appropriately aligned phase). For certain fractional branes the possibility of recombination is not possible, leading to an obstruction to the brane motion.

To conclude this section, we provide an interpretation of the obstruction in terms of the mirror geometry, where a very explicit version of the above picture can be derived. In order to do that, consider the 1-cycles on the mirror Riemann surface Σ which correspond to the different fractional branes, in our case, to the different faces in the dimer. These are sketched in figure 26.

The structure of these 1-cycles, and in particular their winding around the punctures of Σ, leads to a natural explanation of the obstruction. Consider introducing only fractional branes changing the rank of the gauge factor 3. In the mirror this corresponds to

introducing D-branes along the cycle that surrounds the punctures B, C. These punctures end up in different daughter Riemann surfaces in the splitting, see figure 15, hence in trying to perform the partial resolution, the D-brane stretches along the elongated tube, hence increases its tension and breaks supersymmetry. Moreover, it is not possible to express this 1-cycle in terms of a combination of brane cycles not stretching along the tube, hence no process restoring supersymmetry can take place. The same argument goes through if one considers only fractional branes of type 1, since they surround the punctures A, D. Notice that there is no problem if one considers instead fractional branes of type 2 or of type 4, since they do not correspond to cycles stretching along the tube.

Finally, consider introducing the same number of fractional branes of type 1 and 3. This case leads to equal rank for gauge factors 1 and 3, and hence we expect no obstruction. Indeed, although the brane correspond to cycles stretching along the tube, it is possible to deform them topologically to a sum of cycles of type 2 and 4, which do not stretch.

As mentioned above, this picture generalizes to more involved situations. The general lesson is that sets of fractional branes associated to cycles stretching along the tubes which elongate in the factorization of the Riemann surface lead to obstructions to the partial resolution.

4. Complex deformations

In this section we discuss the smoothing of singular geometries via a different process, namely complex deformations. Again, our analysis is general and valid for complex deformations which partially smooth out a singularity, or which split it into two daughter singularities.

Complex deformations of toric singularities have been discussed in diverse contexts. They are easily characterized in terms of the web diagram, as a splitting of the web into two sub-webs in equilibrium. Pictorially, the segment suspended between the two sub-webs after splitting represents the 3-cycle in the deformed geometry. This description, phrased in terms of a physical realization as a fivebrane web in [40, 41] and in toric language in [42, 38], is actually based on the mathematical theory of complex deformations [51 – 53].

In what concerns the relation between complex deformations and the gauge theory on D3-branes, the situation is very different from partial resolutions, and has been studied in [22] (generalizing the conifold case in [4]). The D-branes always live in the resolution phase of the singular geometry. Complex deformation phases are realized after geometric transitions triggered by the back-reaction of a large number of fractional branes.[9] Namely, the homology class wrapped by the fractional brane disappears, and it is replaced by a 3-cycle in a complex deformation phase, which supports 3-form fluxes. This is similar to the Klebanov-Strassler proposal for the conifold with fractional branes [4].

[9]Here by fractional brane we mean any anomaly-free assignment of ranks to the quiver gauge theory, which does not correspond to all factors having equal rank. Also it is important to point out that we center on the case of 'deformation branes' in the sense of [24], since there exist other kinds of fractional branes with different dynamical behaviour, like the removal of supersymmetric vacuum by strong infrared effects [23 – 25], see also [39].

JHEP06(2006)055

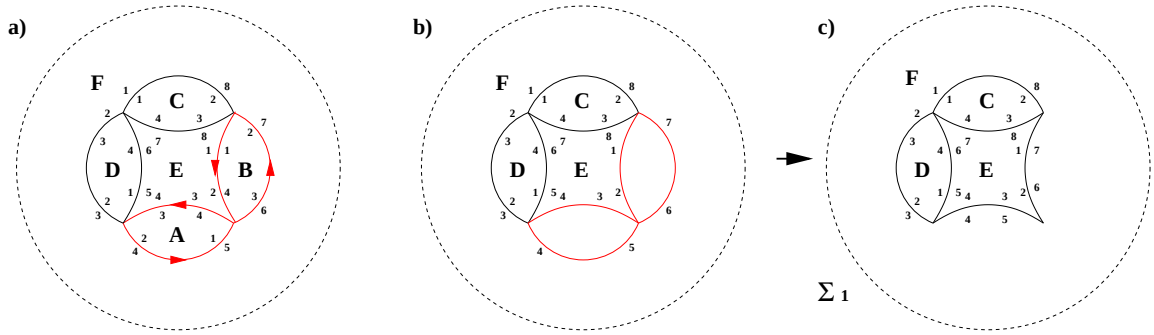

Figure 27: The geometric transition in the mirror picture. (a) the fractional brane defines a 1-cycle in the Riemann surface, along which we cut it (b). Gluing the boundaries of the later gives a daughter Riemann surfaces encoding the mirror geometry of the left over geometry (c).

The description of 'deformation' fractional branes in terms of the dimer diagrams was provided in [24]. Moreover a simple procedure was suggested to transform the original dimer diagram into the dimer diagram of the singular geometry after a complex deformation. Deformation branes correspond to a clusters of faces, touching at their corners, and complex deformation has the effect of smoothing certain touching edges and collapsing the painted regions to zero size. Although efficient, this procedure was rather *ad hoc*, with no derivation from first principles, and no clear rules on which intersections to smooth out, etc. In this section we fill this gap, and find clear rules based on physical principles of geometric transitions.

4.1 An example in the double conifold

Let us start by considering a simple example, namely the complex deformation of the double conifold singularity into a conifold. In order to emphasize the physical ideas, we start with the gauge theory description and derive the effect on the dimer and the description in the web diagram.

Consider the gauge theory for D3-branes at the double conifold singularity (whose dimer diagram is in figure 11) in the presence of additional fractional branes, of the kind that increase the rank of the gauge factor 2. The geometric transition triggered by fractional branes is most easily seen in the mirror picture, in terms of an operation on the mirror Riemann surface. In figure 27a we show the mirror Riemann surface, along with the 1-cycle on which the corresponding fractional brane wraps. It corresponds to a 1-cycle winding around the punctures labeled A and B. The geometric transition corresponds to cutting the Riemann surface along this 1-cycle, as shown in figure 27b, and gluing the boundary to get a new Riemann surface Σ_1, as shown in figure 27c.

Notice that in fact this process leads to to two disjoint Riemann surfaces. The second (denoted Σ_2) corresponds to the removed pieces A, B, with a suitable closing of its boundary. In cases where the 1-cycle splits off two punctures, like in our example, this second Riemann surface is somewhat degenerate and we do not shown it in the pictures.

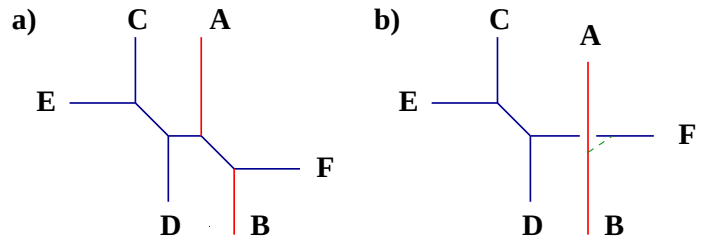

Figure 28: Complex deformation of the double conifold to a conifold singularity.

The distance between the two Riemann surfaces in the ambient space corresponds to the size of the new cycle, which is a 3-cycle in the original D3-brane configuration. The 1-cycle on which the fractional D-branes were wrapping has disappeared as required. The process can be regarded as a splitting of the original web diagram into two sub-webs in equilibrium, given by the sets C, D, E, F and A, B respectively. Hence, from the physics of geometric transitions we recover the usual description in terms of the web diagram as shown in figure 28. A bonus of our argument is that it allows a direct identification of which web splitting corresponds to the geometric transition triggered by a given fractional brane. This piece of the dictionary was missing from previous analysis [22], which supplemented it with suitable guesswork.

The new Riemann surfaces moreover allow us to construct the dimer theories of the theories in the left over geometry after complex deformation. Namely, for each of the Riemann surfaces, the left over zig-zag paths, along with the adjacency relations (including those required by the gluing of boundaries in figure 27), can be used to define the left-over dimer diagram.[10] This is shown in figure 29 for Σ_1. In figure 29a we depict the zig-zag paths of the original dimer diagram which are associated to punctures in the daughter Riemann surface Σ_1. In figure 29b we implement the new adjacency relations implied by the gluing of the boundary in figure 27c. We also show the dimer diagram that corresponds to this final configuration. After integrating out the matter massive due to the bi-valent node, the diagram is easily shown to correspond to the conifold theory, hence describes the gauge theory on D3-branes sitting at the left over conifold singularity after complex deformation.

Notice that this operation on the dimer is equivalent to the proposal in [22] of collapsing some faces to zero, while splitting some nodes open, shown in figure 30. The key difference is that in our analysis the rules are derived from first principles thanks to a proper understanding of the geometric transition and its implications on the dimer.

4.2 An example in dP_3

Let us consider another example, in fact one of the complex deformations discussed in [22].

[10]For Riemann surfaces with two punctures the dimer diagram is somewhat peculiar, with one face, one edge and no nodes. The corresponding gauge theory can however be properly obtained by recalling the physical realization of the dimer in terms of NS- and D5-branes. The special rules for this diagram are due to the extended supersymmetry of the configuration.

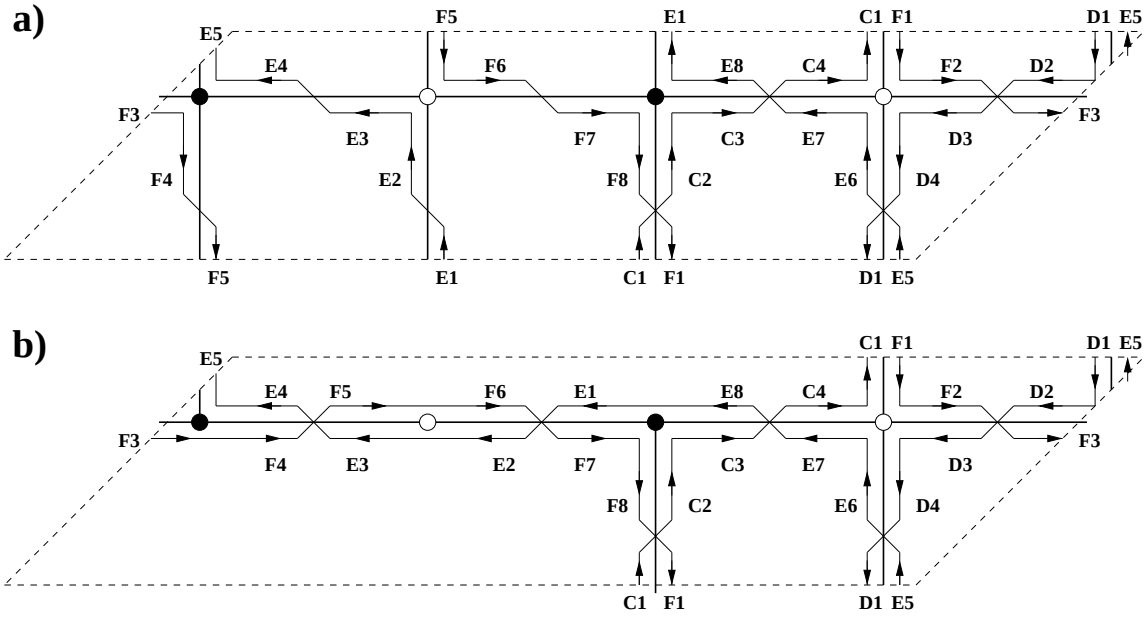

Figure 29: a) Zig-zag paths of the original dimer corresponding to the punctures in Σ_1. b) The closing of the open boundary to get Σ_1 implies adjacency relations that allow to reconstruct the edges of the dimer diagram associated to the D3-branes in the complex deformed geometry. In this case we recover the dimer diagram of a conifold, as expected from a complex deformation of the double conifold.

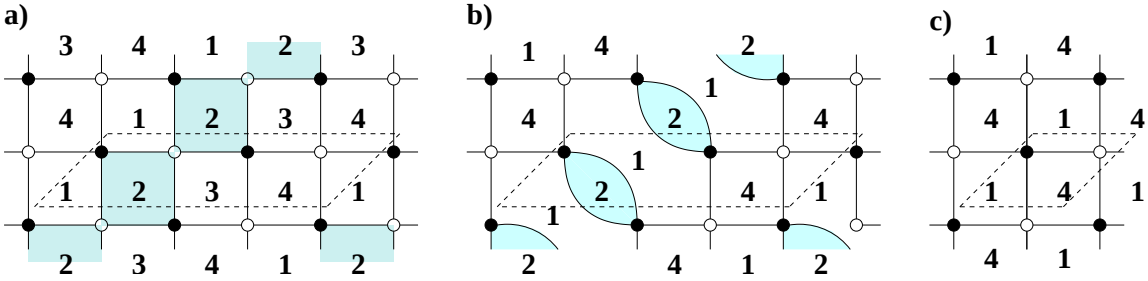

Figure 30: Effect of the complex deformation on the dimer diagram, according to the rules in [22]. (a) shows the fractional branes upon consideration. In (b) the painted areas are contracted, and the nodes where they touched are split open. In (c) we show the contraction of painted regions is completed, leaving a final dimer diagram corresponding to the conifold theory.

Consider the gauge theory on D3-branes at the complex cone over dP_3, whose dimer diagram is shown in figure 20, with a number of fractional branes increasing the rank of the gauge factors 1, 3 and 5 by the same amount. The gauge theory analysis in [22] suggests that these fractional branes trigger a complex deformation smoothing the singularity completely.

We can easily recover this result following the procedure described above in the dimer diagrams. Thus one constructs the 1-cycle in the mirror Riemann surface that is the

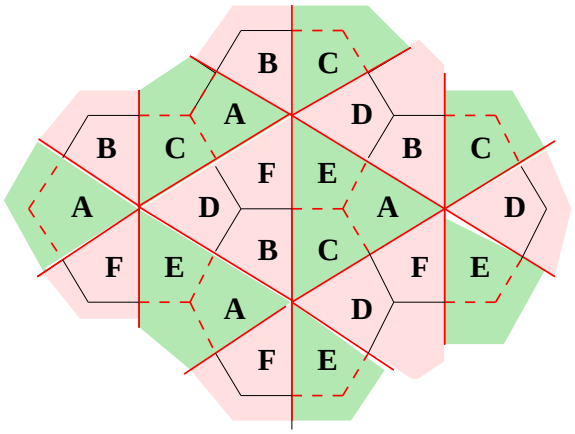

Figure 31: The mirror Riemann surface for dP_3 is a torus with six punctures, which is depicted as a periodic array (the fact that it formally looks like the original dimer diagram is accidental, and not true for a general singularity). The total 1-cycle that corresponds to the fractional brane in the discussion corresponds to a triangular path enclosing the punctures A, C, E, and is shown in red. It separates the Riemann surface in two pieces, shown in different color, each with the topology of a disk.

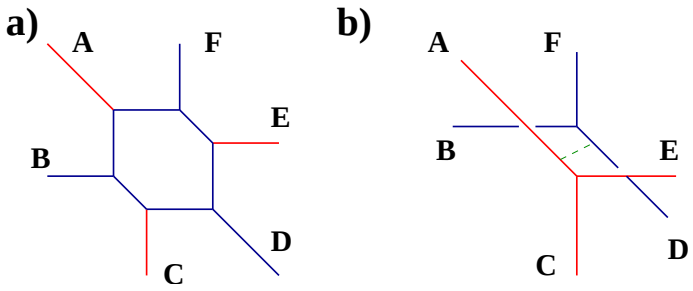

Figure 32: Complex deformation of the cone over dP_3 to a smooth space. The sub-webs describing the left over singularities actually describe two copies of (locally) flat space.

homological sum of the 1-cycles corresponding to the faces 1, 3 and 5. Working this out as in the above example, this total 1-cycle winds around the punctures A, C and E, namely separates the Riemann surface in two regions, which include the punctures A, C, E and B, D, F, respectively. This is shown in figure 31. The geometric transition triggered by the fractional branes should make this cycle disappear, hence we cut the Riemann surface along this cycle, and glue the boundary of each to yield two daughter Riemann surfaces. Each has the topology of a 2-sphere with three punctures. Clearly this process corresponds to a splitting of the web diagram in two sub-webs, in particular to the splitting shown in figure 32. This had already been obtained in [22] by guesswork.

The above operations in the 1-cycles in the mirror Riemann surface, have a direct effect on the set of zig-zag paths of the original theory. In fact, the resulting dimers after the complex deformation can be recovered by directly operating on these. Consider the zig-zag paths of the original dP_3 theory, shown in figure 21. The cutting of the Riemann

JHEP06(2006)055

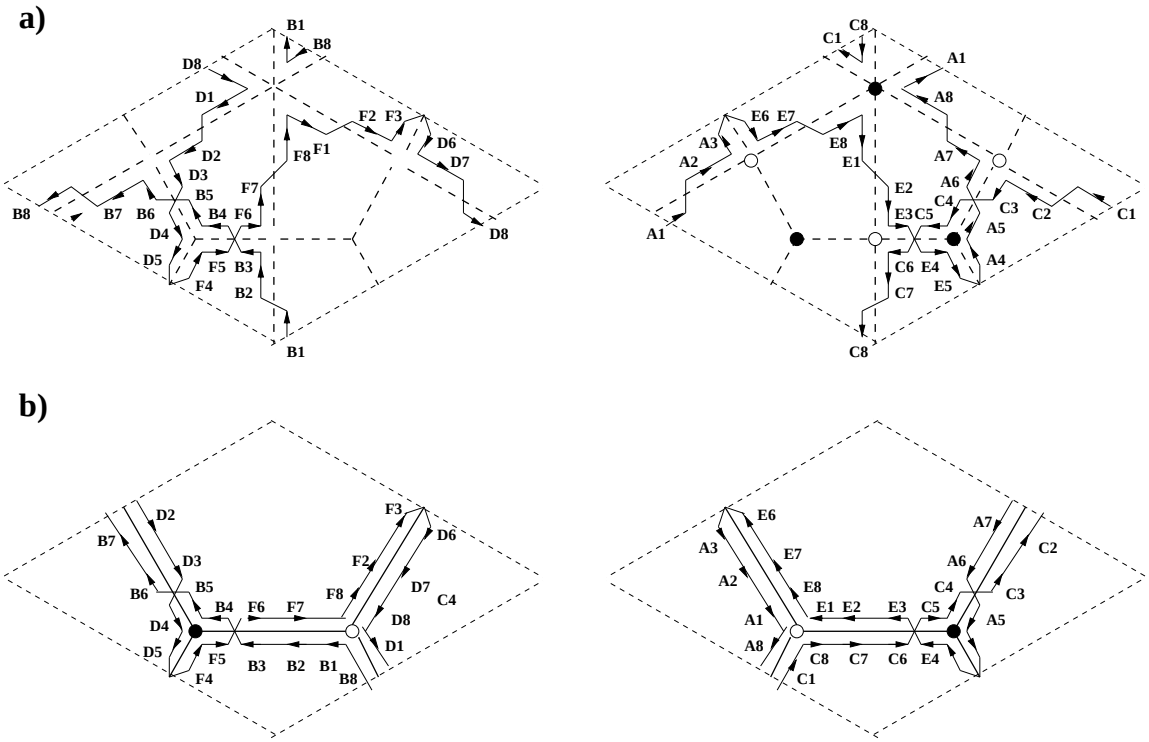

Figure 33: The effect of the complex deformation on the dimer diagram of dP_3. Figure a) shows the two sets of zig-zag paths corresponding to the two pieces of Riemann surface obtained after cutting along the 1-cycle defined by the fractional brane discussed in the main text. Figure b) shows the new zig-zag paths obtained upon imposing the adjacency relations implied by the gluing of boundaries of the Riemann surfaces. Notice these adjacency relations are completely natural from the viewpoint of zig-zag paths; they simply amount to pairing unpaired pieces in a consistent way.

surface separates them into two daughter sets, that will correspond to the zig-zag paths of the daughter theories. They are shown in the figure 33a. The gluing of the boundaries of the pieces of the original Riemann surface to form the daughter ones imply new adjacency relations between the unpaired pieces of the zig-zag paths. The result is two sets of consistent zig-zag paths, which can be used to construct the daughter dimer diagrams. This is shown in figure 33b, where the two daughter dimer diagrams are seen to describe $N = 4$ supersymmetric theories. This corresponds to two sets of D3-branes sitting at different smooth points in the deformed geometry, in agreement with the geometrical picture discussed above.

This example makes manifest one subtle feature. In cutting the Riemann surface, it is not only the homology class of the 1-cycle that is important, rather it is crucial to use the particular representative associated with the tiling of Σ. In the above example the particular representative cuts the Riemann surface into two disks, while a more generic representative in the same homology class (e.g. that obtained by smoothing the intersections in figure 31) would not yield that result.

JHEP06(2006)055

This observation is important in a last respect. It is known that there exist several kinds of fractional branes at singularities, dubbed '$N = 2$', 'deformation' and 'DSB' fractional branes in [24]. Different fractional branes lead to different behaviour of the infrared gauge theory. Interestingly, their differences become manifest in the brane tiling and in the associated 1-cycle in the mirror Riemann surface. Namely, only deformation branes lead to 1-cycles which separate the Riemann mirror surface into two pieces. Hence only deformation branes can lead to a splitting of the Riemann surface making the 1-cycle trivial, as required by the physical interpretation of the geometric transition. For this connection to hold it is crucial *not* to allow to replace the 1-cycle determined by the tiling by another representative in the same homology class.

A last remark is in order. Notice that it is straightforward to derive the rule that complex deformations correspond to splitting off a sub-web in equilibrium. This follows from the fact that the cluster of dimer diagram faces associated to a deformation fractional brane have the topology of a disk. Hence, the total 1-cycle associated to the fractional brane has zero total (p, q) charge. Thus the set of punctures it surrounds, and which correspond to the removed legs in the web diagram, have zero total (p, q) charge, leading to a sub-web in equilibrium.

4.3 Field theory interpretation

The gauge theory interpretation of complex deformations has been discussed for relatively general toric singularities in [22], generalizing the discussion of the conifold in [4]. Complex deformations of the geometry are related to confinement of the gauge factors associated to certain fractional branes. In [22], the appearance of complex deformations in such situations was tested by introducing additional D3-brane probes. Confinement of the fractional brane gauge factors leads to a quantum deformed moduli space for these probes, hence reproducing the complex deformation of the underlying geometry. In fact, if the complex deformed space contains a left over singularity, the gauge theory on the D3-brane probe reduces, after confinement, to the quiver gauge theory associated to that singularity.

In this section we provide a description of the gauge theory analysis of the dynamics of the additional D3-brane probes, along the lines of [22], in terms of dimer diagrams. We show that one can recover the dimer diagram of the left over singularities by simple operations in the dimer, with a clear gauge theory interpretation. Moreover, this recipe agrees with the procedure based on zig-zag paths described in sections 4.1, 4.2.

Let us consider the example in section 4.1 of the double conifold deforming to a conifold. As discussed above, the complex deformation is triggered by introducing fractional branes changing the rank of the gauge factor 2. The complex deformation can be tested by introducing additional D3-branes probes. Hence we consider, as in [22], the gauge theory with rank vector $(M, 2M, M, M)$, and eventually we will focus on $M = 1$.

For convenience we sketch the different steps in the gauge theory analysis (referring the reader to [22] for details), and their implementation in dimer diagrams, as shown in figure 34. The starting dimer diagram with fractional branes is shown for convenience in figure 34a.

JHEP06(2006)055

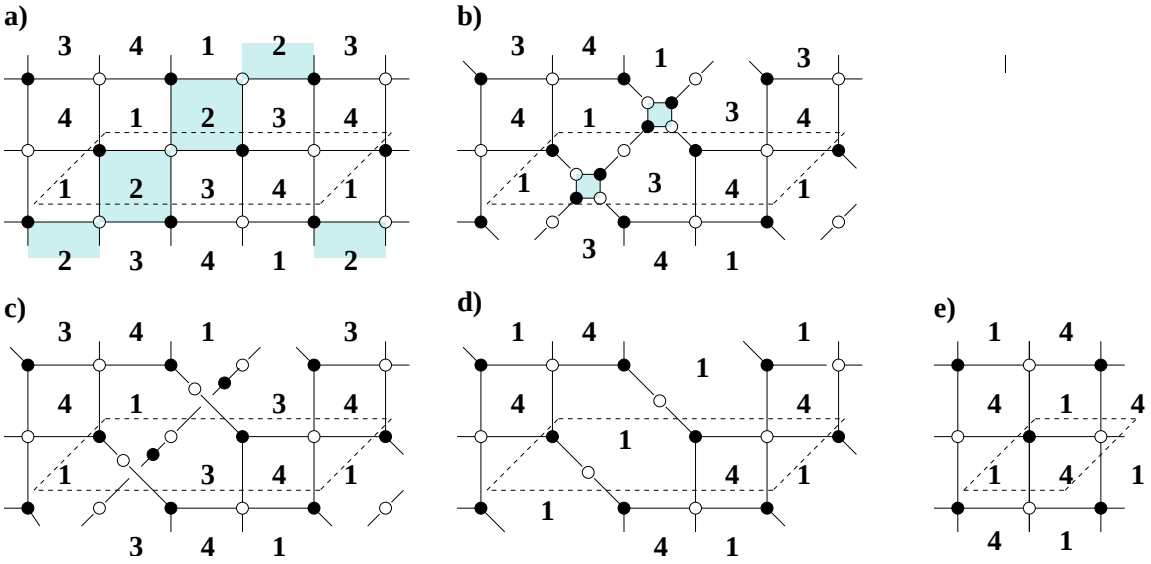

Figure 34: Dimer diagram representation of the gauge theory analysis of D3-branes probing the complex deformation of the double conifold to the conifold. (a) shows the fractional branes upon consideration. In (b) we introduce the mesons of the corresponding gauge factor. In (c) the gauge factor of the fractional branes confines and disappears. They leave behind a non-perturbative contribution to the superpotential of the mesons, implementing their quantum deformed constraint. The fact that the deformed space is not a toric variety is reflected by the fact that the dimer diagram is 'non-planar' with edges passing through each other without intersection. In (d) we show the dimer diagram obtained when some mesons acquire a vev to saturate the quantum constraint. The resulting dimer diagram is equivalent to (e), which corresponds to the conifold theory.

The gauge factor 2 confines, hence one must introduce the corresponding mesons and baryons. The dynamics of the D3-brane probes is manifest on the mesonic branch, so the baryons will play no role and are set to zero. The mesons are however crucial so it is convenient to introduce them in an early stage. Figure 34b shows the gauge theory dimer diagram with the mesons of gauge factor 2 already introduced, even before taking into account the full effects of confinement. The mesons correspond to new edges appearing from the corners of face 2. This intermediate operation is formally similar to the implementation of Seiberg duality in dimer diagrams [27].

Since the gauge factor 2 has the same number of colors and flavours, the classical constraint on the meson matrix has a quantum modification to $\det \mathcal{M} = 1$. This constraint can be implemented in the superpotential via a Lagrange multiplier. Actually, the D3-brane probe theory is manifest when the Lagrange multiplier has actually a non-zero vev. At this stage, all the non-abelian dynamics has been introduced and we can simply consider the abelian situation $M = 1$. In this case, the non-perturbative contribution to the superpotential simply amounts to two quadratic terms in the mesons. The dimer diagram resulting from the above operations is shown in figure 34c. The gauge factor 2 has confined and disappeared. It leaves behind the mesons with new interaction terms between mesons from opposite corners. The latter implies that the diagram cannot be drawn on a torus,

JHEP06(2006)055

since two edges must cross without intersection. This simply reflects the fact that the moduli space of the gauge theory is not a toric variety, in agreement with the fact that a complex deformation of a toric space is not itself a toric space. The dimer diagram clearly knows that after confinement a quantum deformation of the moduli space is taking place!

Although the full deformed geometry is not a toric space, one can zoom into a neighbourhood of the D3-brane probe and find a toric description for it. If one chooses mesonic vevs corresponding to locating the D3-brane probe at the left over singularity in the deformed space, one should then recover the gauge theory of D3-branes at this singularity. At the level of the dimer diagram, a choice of mesonic vevs saturating the constraint $\det \mathcal{M} = 1$ should lead to the dimer diagram of the left over singularity. In figure 34d we show the result of this, where the removal of a line of edges corresponds to giving vevs to the associated mesons. After integrating out the bi-valent nodes, one obtains figure 34e, which corresponds to the dimer diagram of the conifold theory.

Hence, we have provided a set of simple dimer diagram rules which reproduce the gauge theory analysis of the D3-brane probe theory in [22]. Both techniques show that the geometry probed by the D3-brane is the complex deformation of the double conifold to the conifold.

Notice that the gauge theory operations we have just described nicely dovetail the procedure in terms of zig-zag paths described in previous sections. Namely the removal of the sub-web legs corresponds to confinement of the fractional brane. The edges which lose one of their zig-zag paths correspond to fields charged under the fractional brane group, and the process of closing them by new adjacency relations corresponds to constructing the mesons of the confining theory. More precisely, to the mesons that survive after satisfying the quantum constraint via introduction of vevs. Hence, the zig-zag path method provides in one step the final dimer diagram of D3-branes at the left over singularity. Notice also the nice relation between our gauge theory process as described above, and the *ad hoc* dimer diagram rules in [22], see figure 30.

We conclude this section by showing the dimer diagram representation of the gauge theory analysis of D3-branes probes in the complex deformation of the cone over dP_3 to a smooth space. The relevant steps are illustrated in figure 35 and correspond to the gauge theory discussion in section 4.3 in [22]. A sketch of this gauge theory analysis is provided along with the picture. The fact that the dimer diagram rules reproduce in a few easy steps an involved gauge theory analysis, such as this one, illustrates the power of these representations. Moreover, it is easy to show that the complete process is reproduced in a one-step fashion by the operations using zig-zag diagrams described in section 4.2.

4.4 Effect on perfect matchings

In this section we describe complex deformations from another useful viewpoint, in terms of perfect matchings. As we show below, this has a very direct connection with the decomposition of the toric diagram as a Minkowski sum, used in the mathematical literature on complex deformations [51 – 53] (see also appendix in [24] for a short description).

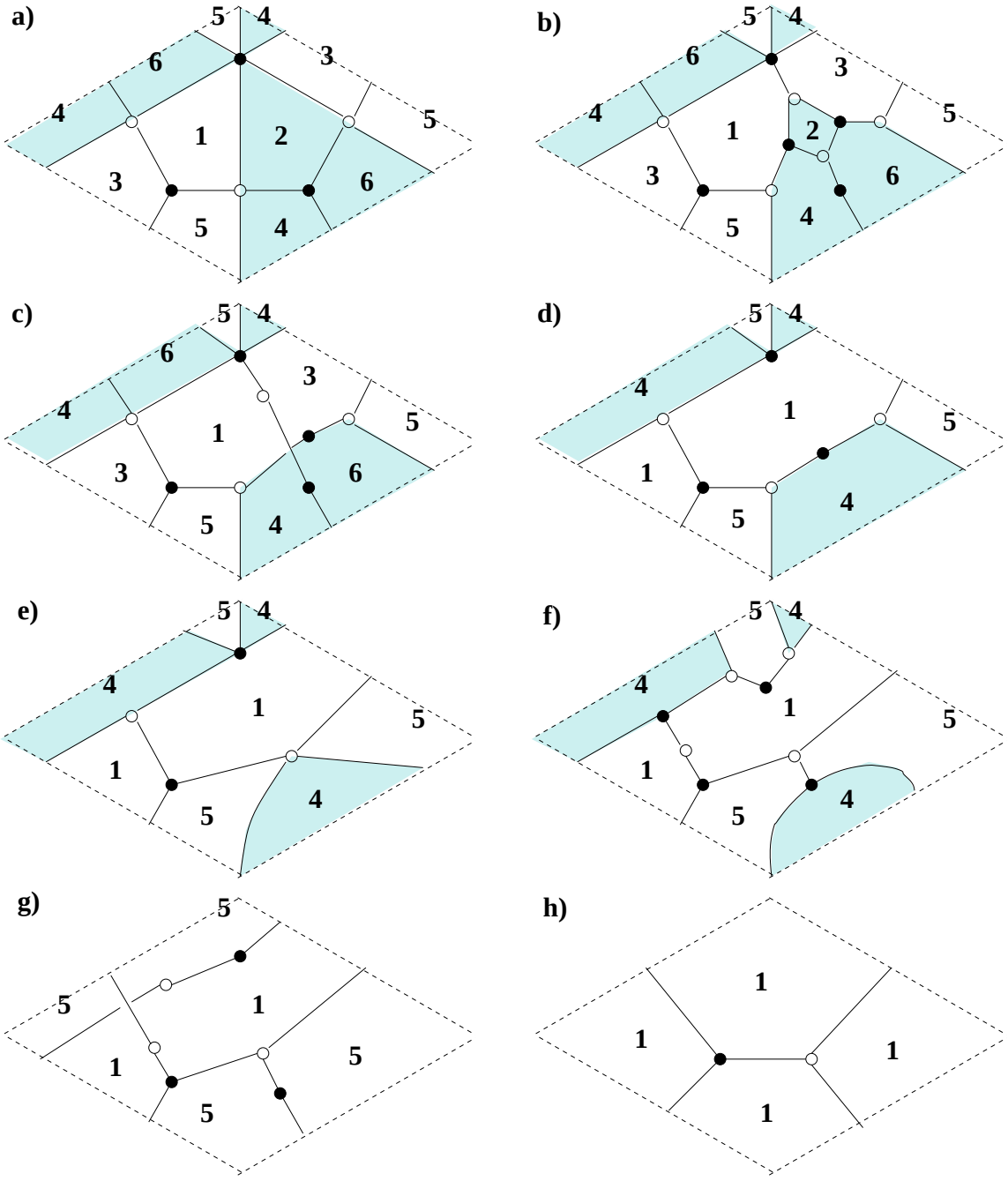

Figure 35: Dimer diagram representation of the gauge theory analysis of D3-branes probing the complex deformation of the cone over dP_3 to a smooth geometry. (a) shows the fractional branes upon consideration. In (b) we introduce the mesons of the gauge factor 2. In (c) the gauge factor 2 confines and induces a non-perturbative superpotential (associated to the quantum constraint on the mesons). In (d) the quantum constraint is saturated by giving vevs to certain mesons, which break the gauge factors 1 and 3, and 4 and 6, to their diagonal combinations, respectively denoted 1 and 4 in the following. After integrating out one bi-valent node (e), the gauge factor 4 has $N_f = N_c$, so we introduce its mesons (f). In (g) the gauge factor 4 confines and induces a non-perturbative superpotential. After giving vevs to some mesons, and integrating out bi-valent nodes, we obtain the dimer diagram (g), corresponding to D3-branes in a smooth geometry.

JHEP06(2006)055

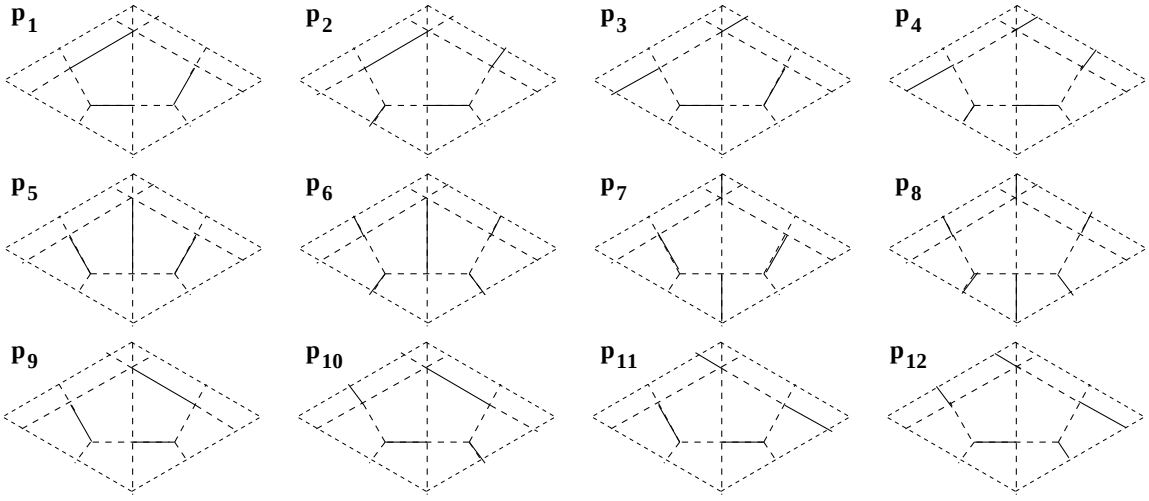

Figure 36: Perfect matchings of the dimer diagram for the dP_3 theory.

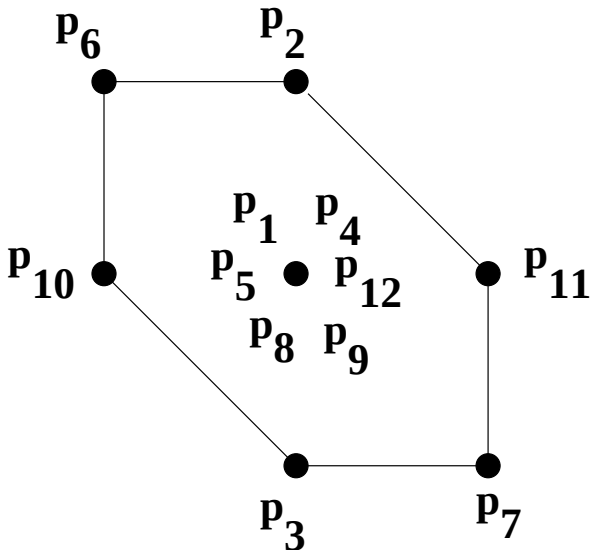

Figure 37: Location of the perfect matchings on the toric diagram for the dP_3 theory.

For concreteness let us consider an example which illustrates the general idea. Consider the deformation of the complex cone over dP_3 to a smooth space, as described in section 4.2. The dimer diagram for the dP_3 theory is shown in figure 20, and its twelve perfect matchings are shown in figure 36.

The location of these perfect matchings in the toric diagram, obtained as described in section 2.3 is shown in figure 37a.

The effect of the complex deformation on the perfect matchings can be determined as follows. Recall that to each pair of perfect matchings we can associated a 1-cycle $p_j - p_i$ in Σ obtained by superimposing them. The complex deformation amounts to cutting Σ in

two pieces and gluing the boundary of each piece separately to obtain Σ_1 and Σ_2. In this process, some of the homology classes of Σ become trivial in e.g. Σ_1. This implies non-trivial equivalence relations between difference paths of perfect matchings. For instance, matchings whose difference path is a combination of the 1-cycles becoming trivial become equivalent in Σ_1. In addition to these identifications, the equivalence relations also imply changes in the slopes of the matchings, and thus an induced change in the toric diagram.

To illustrate the procedure let us consider the deformation of the complex cone over dP_3 to a smooth space. In this example, studied above, Σ_1 is obtained by removing the zig-zag paths A, C, E, enclosed by the fractional brane associated to the gauge factors 2, 4, 6. It is easy to obtain the fate of the different 1-cycles of Σ in Σ_1, by drawing them on the Riemann surface. For instance, the zig-zag paths A, C, E become trivial in Σ_1, whereas B, D, F remain non-trivial zig-zag paths in the daughter surface. Another interesting set of 1-cycles is given by those associated to the i^{th} gauge factor, which we denote by f_i. One can check that f_2, f_4, f_6 become trivial in Σ_1, while f_1, f_3, f_5 become identical to $-$B, $-$D, $-$F in Σ_1. Then one can easily check relations like $p_1 - p_3 = -A - E + f_2 \simeq 0$, etc. Following this, the matchings fall into three equivalence classes. We have

$$p_1 = p_3 = p_{10} = p_{12}\,; \qquad p_2 = p_4 = p_6 = p_8\,; \qquad p_5 = p_7 = p_9 = p_{11} \tag{4.1}$$

In addition one can obtain relations like $p_1 - p_2 = F + f_2 \simeq F$, etc, which can be used to obtain the new relative slopes, and the positions of the (equivalence classes of) perfect matchings in the new toric diagram. The result of this operation is shown in figure 38a. The result is indeed the diagram corresponds to a smooth space, in fact the dual to the subweb corresponding to the legs B, D, F. The resulting diagram can be regarded as a contraction of the original toric diagram along a triangle, as illustrated in figure 38b.

Clearly, one can operate in a similar manner with the other daughter Riemann surface Σ_2, and define another set of equivalences of perfect matchings. The end result is that the equivalence classes describe a toric diagram dual to the sub-web diagram corresponding to the legs A, C, E, as expected for Σ_2.

The splitting of the toric diagram into several sub-diagrams is dual to the splitting of the web diagram into sub-webs in equilibrium. Now the splitting of the toric diagram into sub-diagrams, each of which can be regarded as a contraction of the initial diagram (along the other sub-diagrams) has a nice connection with the mathematical operation known as decomposition of a toric polygon into Minkowski summands [51 – 53]. In fact, this operation lies at the heart of the mathematical characterization of complex deformations of toric singularities. It is a pleasant surprise to find a direct realization of the Minkowski decomposition of the toric diagram in the dimer language. We hope this relation brings the mathematics literature somewhat closer to the physical realization of deformations via geometric transitions (see [54] for an example of this).

As a final remark, we would like to point out that the use of perfect matchings also provides an interesting new way to recover the dimer diagrams of the daughter theories. Namely, after determining the equivalence classes of perfect matchings for a given Riemann surface, one can pick one representative of each class, and consider the set of edges involved

JHEP06(2006)055

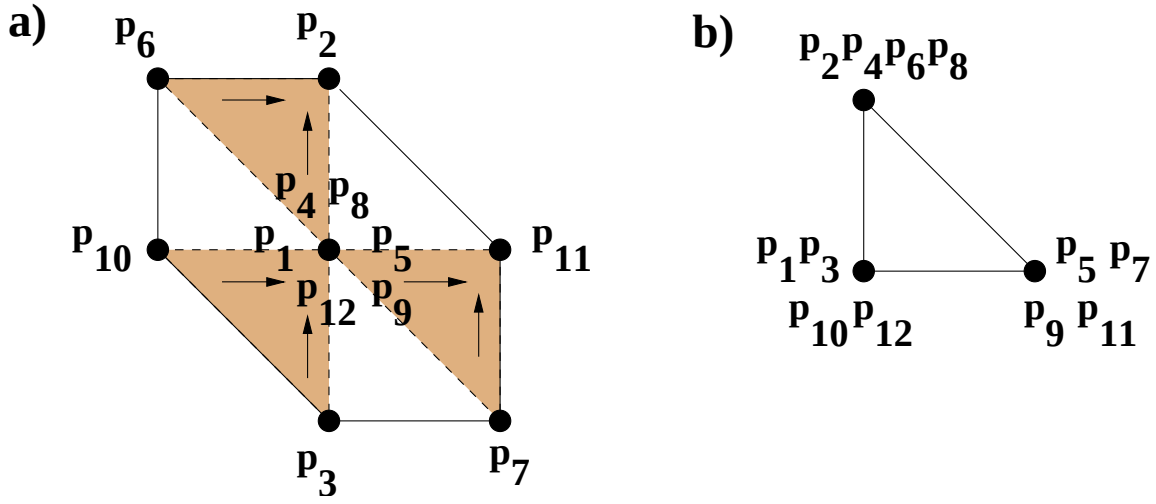

Figure 38: a) The location of the equivalence classes of matchings describes the toric diagram of the first daughter geometry. In this case we recover the toric diagram of a smooth space, precisely the dual of the sub-web diagram corresponding to the legs B, D, F in figure 32. Notice that all matchings in each vertex are equivalent (so their real multiplicity in the toric diagram is 1. b) The equivalence relation between perfect matchings can be regarded as the contraction of certain triangles in the toric diagram.

in this set of matchings. The diagram obtained by superimposing all of them is exactly the dimer diagram that corresponds to the daughter theory.

5. Conclusions

In this paper we have provided tools to describe in full generality the processes that smooth out toric singularities, from the viewpoint of the gauge theory on D3-branes probing such geometries. The results are nicely cast in the language of dimer diagrams, in particular making use of the connection between the dimer diagram and the web diagram (via zig-zag paths and/or perfect matchings).

For partial resolutions our tools should allow a quick construction of the gauge theory for any toric singularity. It would suffice to implement out optimized tools using zig-zag paths to the partial resolution algorithm introduced in [7], with the advantage of being able to carry out a complicated partial resolution in one step.

We have also provided a detailed gauge theory interpretation of the splitting of a dimer diagram into sub-dimers in the partial resolution process. It corresponds to a specific Higgs mechanism which splits the gauge theory into two gauge sectors decoupled at the level of massless states. We envision interesting model building applications of such systems.

An interesting open question is to understand the inverse process of combining different toric singularities into a single one, by inverting the partial resolution. Namely, by adjoining the corresponding web diagrams along one or several legs, and to shrink the resulting

segments. Progress in this direction should deal with ambiguities in the precise dimer diagrams to be combined, since the latter are defined modulo integration of bi-valent nodes.

For complex deformations we have provided a dictionary between the fractional branes and the precise splitting of the web diagram into sub-webs. Moreover, we have provided a simple set of dimer rules that reproduce the involved non-perturbative gauge theory analysis which describes D3-branes probes at such geometries. In addition the net result of these gauge theory operations is subsumed in extremely simple operations on the dimer in terms of zig-zag paths. It would be interesting to develop similar tools to analyze other infrared behaviours, like the removal of the supersymmetric vacuum by DSB branes.

We hope these tools are useful for these and other interesting purposes.

Acknowledgments

We thank S. Franco and A. Hanany for illuminating conversations. A.M.U. thanks M. González for kind encouragement and support. F.S. and I.G.-E. thank CERN TH for hospitality during completion of this project. This work has been partially supported by CICYT (Spain) under project FPA-2003-02877, and the RTN networks MRTN-CT-2004-503369 'The Quest for Unification: Theory confronts Experiment', and MRTN-CT-2004-005104 'Constituents, Fundamental Forces and Symmetries of the Universe'. The research of F.S. is supported by the Ministerio de Educación y Ciencia through an F.P.U grant. The research of I.G.-E. is supported by the Gobierno Vasco PhD fellowship program and the Marie Curie EST program.

A. Proof of flatness

The flatness conditions can be checked in the general case, by a slight generalization of the analysis in the example in section 3.3. We recall that in this section we are considering original dimer diagrams not containing bi-valent nodes (hence they have been integrated out if originally present).

F-flatness conditions. As described in section 3.4, in partial resolutions each subdimer contains at least one perfect matching of the original dimer diagram. This implies that every sub-dimer contains all the nodes of the original dimer diagram. From this follows that in any sub-dimer, for any node there are at least two edges ending on it in every sub-dimer. At the level of the gauge theory, this implies that for each superpotential term of the original theory there are a sufficient number of bi-fundamentals with zero vevs to automatically satisfy the F-term conditions. Hence the assignment of vevs dictated by the dimer rules is F-flat.

Non-abelian D-flatness conditions. As described in section 3, we divide the set of zig-zag paths into two disjoint sets, where each set admits a dual interpretation as the set of external legs in the web diagram that we take to infinity. Let us denote collectively the elements belonging to the first set as 1 and those belonging to the other set as 2.

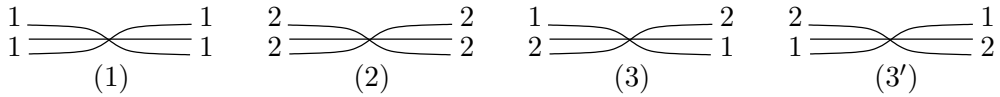

Figure 39: The four possible types of edges, classified according to the zig-zag paths meeting at the edge.

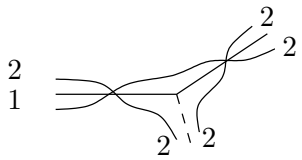

Figure 40: Inconsistent pasting of edges (3′2). Note that the only constraints come from the joining of the interior zig-zag paths. The exterior ones can be arbitrary as they do not need to be joined (in the absence of bi-valent nodes) since they "run off" along some extra edge, denoted by the dashed line in the drawing.

Consider a given face in the dimer diagram, and orient its edges by running through them e.g. counterclockwise. Each edge can then be classified into 4 types depending on which kind of zig-zag paths intersect over it. We will denote the four kinds as type 1, 2, 3 and 3′, see figure 39, where 3 and 3′ are distinguished by the orientation.[11]

In this fashion, we assign to each face a (periodic) string of symbols given by the kind of edges we encounter when traversing the face counterclockwise. A typical string will then look like:

$$\ldots 3'1323'3\ldots$$

where we have written just the period. It is easy to realize that any valid string should satisfy a few rules which we can read from the dimer diagram. Namely there are some sequences of symbols that are not allowed, for example 3′2. To see this, focus on the zig-zag paths "interior" to the edge. The given sequence would tell us that a type 1 zig-zag path exits the 3′ vertex from the right, and then joins a type 2 zig-zag path in the next edge, see figure 40. This is obviously not allowed. The other disallowed sequences are 13′, 23, 31, 33, 3′3′, 12 and 21.

We can then associate to the most general face in a dimer a sequence of symbols not containing these forbidden words. It is easy to convince oneself that in any such string, at least one of the following substitutions applies and gives rise to another consistent sequence with two symbols removed in the period ("·" denotes the empty word):

$$\begin{aligned} &11 \longrightarrow \cdot\,; \qquad 22 \longrightarrow \cdot\,; \qquad 33' \longrightarrow \cdot\,; \qquad 3'3 \longrightarrow \cdot \\ &132 \longrightarrow 3\,; \qquad 23'1 \longrightarrow 3' \end{aligned}$$

[11] The similar notation for edges and zig-zag paths is introduced to (hopefully) improve the readability. In the rest of this section we mostly deal with edges, so this should not cause too much confusion.

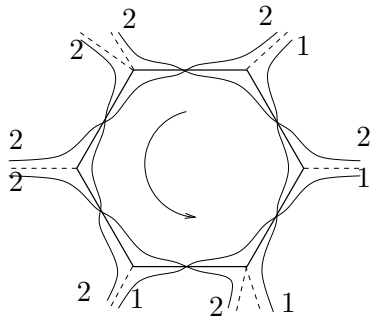

Figure 41: A possible face in a dimer, where we have indicated the relevant classification for the zig-zag paths. External edges are denoted by the dashed lines, and the arrow indicates the traversal direction used in the text when enumerating the edges.

As an example, applying the rules one would get the following sequence of strings:

$$3'133'1132 \longrightarrow 3'11132 \longrightarrow 3'132 \longrightarrow 3'3 \longrightarrow \cdot$$

Since we can always apply one of these rules, and all of them reduce the length of the string by two, we have found that it is always possible to reduce an arbitrary string to nothing.[12] The interesting fact about these operations is that on the field theory side they do not change the value of the D-term. Essentially, the first four rules preserve the D-term value because the disappeared edges correspond to a fundamental and an antifundamental with the same vev, hence with canceling contributions to the D-term. For the last two rules, the disappeared edges have vevs whose contributions add up to the trace of an SU(N) generator, which is zero. One can in this way easily translate between the language used in equation 3.4 and this language of sequences. What this means is that the value of the D-term for all possible faces in a dimer is given by the D-term of the empty sequence, which is equal to zero.

As an example, let us study the configuration depicted in figure 41. The periodic string we associate with the face is given by $\ldots 223'132\ldots$. Applying the rules we have described a possible reduction to nothing would be:

$$223'132 \longrightarrow 23'32 \longrightarrow 22 \longrightarrow \cdot$$

This proves that the D-term for the relevant gauge group vanishes.

References

[1] M.R. Douglas and G.W. Moore, *D-branes, quivers and ALE instantons*, `hep-th/9603167`.

[2] M.R. Douglas, B.R. Greene and D.R. Morrison, *Orbifold resolution by D-branes*, *Nucl. Phys.* **B 506** (1997) 84 [`hep-th/9704151`].

[3] I.R. Klebanov and E. Witten, *Superconformal field theory on threebranes at a Calabi-Yau singularity*, *Nucl. Phys.* **B 536** (1998) 199 [`hep-th/9807080`].

[12] The sequences always have even length, consistently with anomaly cancellation.

[4] I.R. Klebanov and M.J. Strassler, *Supergravity and a confining gauge theory: duality cascades and χSB-resolution of naked singularities*, *JHEP* **08** (2000) 052 [hep-th/0007191].

[5] M. Wijnholt, *Large volume perspective on branes at singularities*, *Adv. Theor. Math. Phys.* **7** (2004) 1117 [hep-th/0212021].

[6] C.P. Herzog, *Exceptional collections and del Pezzo gauge theories*, *JHEP* **04** (2004) 069 [hep-th/0310262].

[7] D.R. Morrison and M.R. Plesser, *Non-spherical horizons, I*, *Adv. Theor. Math. Phys.* **3** (1999) 1 [hep-th/9810201]; [8].

[8] C. Beasley, B.R. Greene, C.I. Lazaroiu and M.R. Plesser, *D3-branes on partial resolutions of abelian quotient singularities of Calabi-Yau threefolds*, *Nucl. Phys.* **B 566** (2000) 599 [hep-th/9907186].

[9] B. Feng, A. Hanany and Y.-H. He, *D-brane gauge theories from toric singularities and toric duality*, *Nucl. Phys.* **B 595** (2001) 165 [hep-th/0003085].

[10] A. Hanany and A. Iqbal, *Quiver theories from D6-branes via mirror symmetry*, *JHEP* **04** (2002) 009 [hep-th/0108137].

[11] B. Feng, A. Hanany, Y.H. He and A. Iqbal, *Quiver theories, soliton spectra and Picard-Lefschetz transformations*, *JHEP* **02** (2003) 056 [hep-th/0206152].

[12] B. Feng, S. Franco, A. Hanany and Y.-H. He, *Unhiggsing the del Pezzo*, *JHEP* **08** (2003) 058 [hep-th/0209228].

[13] A. Hanany, P. Kazakopoulos and B. Wecht, *A new infinite class of quiver gauge theories*, *JHEP* **08** (2005) 054 [hep-th/0503177].

[14] M. Bertolini, F. Bigazzi and A.L. Cotrone, *New checks and subtleties for AdS/CFT and a-maximization*, *JHEP* **12** (2004) 024 [hep-th/0411249].

[15] S. Benvenuti, S. Franco, A. Hanany, D. Martelli and J. Sparks, *An infinite family of superconformal quiver gauge theories with Sasaki-Einstein duals*, *JHEP* **06** (2005) 064 [hep-th/0411264].

[16] S. Benvenuti and M. Kruczenski, *From Sasaki-Einstein spaces to quivers via BPS geodesics: $L(p,q|r)$*, *JHEP* **04** (2006) 033 [hep-th/0505206].

[17] S. Franco, A. Hanany, D. Martelli, J. Sparks, D. Vegh and B. Wecht, *Gauge theories from toric geometry and brane tilings*, *JHEP* **01** (2006) 128 [hep-th/0505211].

[18] A. Butti, D. Forcella and A. Zaffaroni, *The dual superconformal theory for $L(p,q,r)$ manifolds*, *JHEP* **09** (2005) 018 [hep-th/0505220].

[19] A. Butti and A. Zaffaroni, *R-charges from toric diagrams and the equivalence of a-maximization and z-minimization*, *JHEP* **11** (2005) 019 [hep-th/0506232].

[20] S. Franco, Y.-H. He, C. Herzog and J. Walcher, *Chaotic duality in string theory*, *Phys. Rev.* **D 70** (2004) 046006 [hep-th/0402120].

[21] C.P. Herzog, Q.J. Ejaz and I.R. Klebanov, *Cascading RG flows from new Sasaki-Einstein manifolds*, *JHEP* **02** (2005) 009 [hep-th/0412193].

[22] S. Franco, A. Hanany and A.M. Uranga, *Multi-flux warped throats and cascading gauge theories*, *JHEP* **09** (2005) 028 [hep-th/0502113].

JHEP06(2006)055

[23] D. Berenstein, C.P. Herzog, P. Ouyang and S. Pinansky, *Supersymmetry breaking from a Calabi-Yau singularity*, *JHEP* **09** (2005) 084 [hep-th/0505029].

[24] S. Franco, A. Hanany, F. Saad and A.M. Uranga, *Fractional branes and dynamical supersymmetry breaking*, *JHEP* **01** (2006) 011 [hep-th/0505040].

[25] M. Bertolini, F. Bigazzi and A.L. Cotrone, *Supersymmetry breaking at the end of a cascade of Seiberg dualities*, *Phys. Rev.* **D 72** (2005) 061902 [hep-th/0505055].

[26] A. Hanany and K.D. Kennaway, *Dimer models and toric diagrams*, hep-th/0503149.

[27] S. Franco, A. Hanany, K.D. Kennaway, D. Vegh and B. Wecht, *Brane dimers and quiver gauge theories*, *JHEP* **01** (2006) 096 [hep-th/0504110].

[28] A. Hanany and D. Vegh, *Quivers, tilings, branes and rhombi*, hep-th/0511063.

[29] B. Feng, Y.-H. He, K.D. Kennaway and C. Vafa, *Dimer models from mirror symmetry and quivering amoebae*, hep-th/0511287.

[30] S. Franco and D. Vegh, *Moduli spaces of gauge theories from dimer models: proof of the correspondence*, hep-th/0601063.

[31] C.E. Beasley and M.R. Plesser, *Toric duality is Seiberg duality*, *JHEP* **12** (2001) 001 [hep-th/0109053].

[32] B. Feng, A. Hanany, Y.-H. He and A.M. Uranga, *Toric duality as Seiberg duality and brane diamonds*, *JHEP* **12** (2001) 035 [hep-th/0109063].

[33] D. Berenstein and M.R. Douglas, *Seiberg duality for quiver gauge theories*, hep-th/0207027.

[34] C.P. Herzog, *Seiberg duality is an exceptional mutation*, *JHEP* **08** (2004) 064 [hep-th/0405118].

[35] A. Hanany, C.P. Herzog and D. Vegh, *Brane tilings and exceptional collections*, hep-th/0602041.

[36] C. Vafa, *Superstrings and topological strings at large-N*, *J. Math. Phys.* **42** (2001) 2798 [hep-th/0008142].

[37] F. Cachazo, B. Fiol, K.A. Intriligator, S. Katz and C. Vafa, *A geometric unification of dualities*, *Nucl. Phys.* **B 628** (2002) 3 [hep-th/0110028].

[38] M. Aganagic and C. Vafa, *G_2 manifolds, mirror symmetry and geometric engineering*, hep-th/0110171.

[39] K. Intriligator and N. Seiberg, *The runaway quiver*, *JHEP* **02** (2006) 031 [hep-th/0512347].

[40] O. Aharony and A. Hanany, *Branes, superpotentials and superconformal fixed points*, *Nucl. Phys.* **B 504** (1997) 239 [hep-th/9704170].

[41] O. Aharony, A. Hanany and B. Kol, *Webs of (p,q) 5-branes, five dimensional field theories and grid diagrams*, *JHEP* **01** (1998) 002 [hep-th/9710116].

[42] N.C. Leung and C. Vafa, *Branes and toric geometry*, *Adv. Theor. Math. Phys.* **2** (1998) 91 [hep-th/9711013].

[43] R. Kenyon, *An introduction to the dimer model*, math.CO/0310326.

[44] R. Kenyon and J.-M. Schlenker *Rhombic embeddings of planar graphs with faces of degree 4*, *Trans. Amer. Math. Soc.***357** (2005) 3443 [math-ph/0305057].

JHEP06(2006)055

[45] A. Hanany and A. Zaffaroni, *On the realization of chiral four-dimensional gauge theories using branes*, *JHEP* **05** (1998) 001 [hep-th/9801134].

[46] A. Hanany, M.J. Strassler and A.M. Uranga, *Finite theories and marginal operators on the brane*, *JHEP* **06** (1998) 011 [hep-th/9803086].

[47] A. Hanany and A.M. Uranga, *Brane boxes and branes on singularities*, *JHEP* **05** (1998) 013 [hep-th/9805139].

[48] M. Aganagic, A. Karch, D. Lüst and A. Miemiec, *Mirror symmetries for brane configurations and branes at singularities*, *Nucl. Phys.* **B 569** (2000) 277 [hep-th/9903093].

[49] A.M. Uranga, *Brane configurations for branes at conifolds*, *JHEP* **01** (1999) 022 [hep-th/9811004].

[50] L.E. Ibáñez, R. Rabadán and A.M. Uranga, *Anomalous* U(1)*'s in type-I and type-IIB* $D = 4$, $N = 1$ *string vacua*, *Nucl. Phys.* **B 542** (1999) 112 [hep-th/9808139].

[51] K. Altmann, *The versal deformation of an isolated toric Gorenstein singularity*, alg-geom/9403004.

[52] K. Altmann, *Infinitesimal deformations and obstructions for toric singularities*, alg-geom/9405008.

[53] K. Altmann, *Deformations of toric singularities*, Habilitationsschrift, Humboldt-Universität zu Berlin 1995, available at http://page.mi.fu-berlin.de/~altmann/PAPER/.

[54] S. Pinansky, *Quantum deformations from toric geometry*, *JHEP* **03** (2006) 055 [hep-th/0511027].

JHEP06(2006)055